Myeloid Cells

Science Exploration

Open Access Research Article

Scalable generation of pure CD103$^+$ cDC1 from iDC1 cultures

Sukriti Sharma[1], Fiona Flynn[1], Brian Capaldo[2], Ronald Holewinski[3], Qingrong Chen[2], Daoud Meerzaman[2], Thorkell Andresson[3], Christian T. Mayer[1,*]

[1]Experimental Immunology Branch, Center for Cancer Research, National Cancer Institute, National Institutes of Health, Bethesda, MD 20892, USA.
[2]Computational Genomics and Bioinformatics Branch, National Cancer Institute, National Institutes of Health, Frederick, MD 20850, USA.
[3]Protein and Metabolite Characterization Core, Cancer Research and Technology Program, Frederick National Laboratory for Cancer Research, National Institutes of Health, Frederick, MD 21701, USA.

***Correspondence to:** Christian T. Mayer, Experimental Immunology Branch, Center for Cancer Research, National Cancer Institute, National Institutes of Health, Bethesda, MD 20892, USA. E-mail: christian.mayer@nih.gov

Received: June 04, 2026 **Accepted:** August 28, 2026 **Published:** August 28, 2026

Cite this article: Sharma S, Flynn F, Capaldo B, Holewinski R, Chen Q, Meerzaman D, et al. Scalable generation of pure CD103+ cDC1 from iDC1 cultures. Myeloid Cells. 2026;1:202613. https://doi.org/10.70401/mc.2026.0012

Abstract

Aims: Conventional type 1 dendritic cells (cDC1) specialize in cross-presentation and interleukin-12 production and are critical for immunity against intracellular pathogens and tumors, but remain rare *in vivo*, limiting mechanistic and translational studies. Existing bone marrow-derived dendritic cell (BMDC) methods do not achieve selective enrichment of cDC1 or scalable production at high purity. We therefore aimed to establish a high-efficiency BMDC culture system for selective generation of CD103$^+$ cDC1 from mouse bone marrow.

Methods: Mouse bone marrow cells were cultured in defined medium with recombinant fms-like tyrosine kinase 3 ligand (FLT3L), low-dose granulocyte-macrophage colony-stimulating factor (GM-CSF), and Kit ligand (KitL) to generate induced cDC1 (iDC1). Phenotypic, transcriptomic, proteomic, phospho-proteomic, and functional analyses were performed and compared with established BMDC methods and *ex vivo* immune cell populations.

Results: iDC1 cultures enabled scalable generation of an estimated 1.5 × 10^9 CD103$^+$ cDC1 at greater than 95% purity from a single mouse, representing at least a 75-fold increase relative to previous recombinant cytokine-based methods. iDC1 closely aligned with the cDC1 lineage while distinct from macrophages. Functionally, iDC1 responded robustly to innate stimulation, secreted interleukin 12 (IL-12)p40 and inflammatory chemokines, and efficiently cross-presented cell-associated antigen to CD8$^+$ T cells. Mechanistically, KitL and GM-CSF cooperated during early cDC1 generation, whereas GM-CSF promoted proliferation and survival during later stages of culture. iDC1 generation depended on the +32 kb *Irf8* enhancer, and signal transducer and activator of transcription 5 (STAT5)- and bromodomain-containing protein 4 (BRD4)-associated regulatory programs contributed to efficient iDC1 generation.

Conclusion: iDC1 cultures are a scalable platform for studying cDC1 biology and may facilitate development and preclinical evaluation of cDC1-based immunotherapeutic strategies.

Keywords: iDC1, cDC1, CD103+ DC, GM-CSF, cross-presentation, STAT5, BRD4, IL-12p40

1. Introduction

Dendritic cells (DCs) comprise conventional DCs (cDCs) and plasmacytoid DCs (pDCs). Two major cDC subsets, cDC1 and cDC2, populate both lymphoid and non-lymphoid tissues and can be broadly classified as resident or migratory cDC, respectively[1]. Conventional type 1 dendritic cells (cDC1) specialize in the cross-presentation of cell-associated antigens, produce interleukin-12 (IL-12) following toll-like receptor (TLR) 3, TLR11 and TLR12 activation, and orchestrate adaptive immune responses to intracellular pathogens and tumors[2-7]. Significant progress has been made in defining the transcriptional network controlling cDC1 lineage specification. In particular, transcription factor interferon regulatory factor 8 (IRF8) is essential for cDC1 lineage development through formation of complexes with basic leucine zipper transcription factors BATF, BATF2 or BATF3 together with Jun proteins, resulting in IRF8 autoactivation at the +32 kb *Irf8* enhancer[8,9]. Mice lacking the +32 kb *Irf8* enhancer (*Irf8*$^{+32-/-}$) completely lack cDC1 under both steady-state and inflammatory conditions[10].

Because DCs, and particularly cDC1, are rare *in vivo*, bone marrow-derived DC (BMDC) culture systems have become invaluable tools for studying DC development, biology, and therapeutic potential[11]. Culture of bone marrow cells with granulocyte-macrophage colony-stimulating factor (GM-CSF) generates macrophages (GM-Mac) and DC (GM-DC)-like cells that do not clearly correspond to cDC1 or cDC2 populations found *in vivo*[12-14]. In contrast, fms-like tyrosine kinase 3 ligand (FLT3L)-driven cultures (FLT3L-DC) generate

© The Author(s) 2026. This is an Open Access article licensed under a Creative Commons Attribution 4.0 International License (https://creativecommons.org/licenses/by/4.0/), which permits unrestricted use, sharing, adaptation, distribution and reproduction in any medium or format, for any purpose, even commercially, as long as you give appropriate credit to the original author(s) and the source, provide a link to the Creative Commons license, and indicate if changes were made.

all major DC subsets, including pDCs, cDC1 and cDC2[15,16].

Recent efforts have focused on selectively biasing BMDC differentiation toward cDC1[17-20] or cDC2[21], which could greatly facilitate basic and pre-clinical research by increasing DC subset yield and purity while potentially circumventing the need for magnetic enrichment or fluorescence-activated cell sorting. Low-dose GM-CSF combined with FLT3L strongly biases iCD103-DC cultures toward cDC1 production[19]. Kit ligand (KitL)/stem cell factor, interleukin-4 (IL-4), and OP9 stromal cells have also been reported to enhance FLT3L-dependent cDC1 generation[17,18,20]. However, currently available methods do not achieve highly selective cDC1 production above 95% purity at scalable yield. Importantly, BMDC purity should not be assessed solely within gated DC populations, because the frequency of individual DC subsets within the DC compartment does not necessarily reflect the overall composition of the culture. Instead, BMDC purity must also account for macrophage and other non-DC contaminants contributing to culture heterogeneity.

Here, we describe a 23-day BMDC method termed induced cDC1 (iDC1) that uses recombinant cytokines to generate approximately 1.5×10^9 $CD103^+$ cDC1 at greater than 95% purity from a single mouse. We further show that iDC1 exhibit key phenotypic, transcriptional, and functional features of the cDC1 lineage and identify GM-CSF-regulated signaling and regulatory programs that promote efficient cDC1 generation and maintenance in iDC1 cultures. These findings establish iDC1 cultures as a scalable platform for studying cDC1 biology and therapeutic potential.

2. Methods

2.1 Mice

C57BL/6J (Strain #000664), C57BL/6-Irf8em1Kmm/J (*Irf8*$^{+32-/-}$; Strain #032744)[10], B6N(129S4)-Xcr1tm1.1(cre)Kmm/J ($Xcr1^{Cre}$; Strain #035435)[22], and B6.C-Tg(CMV-cre)1Cgn/J (CMV^{Cre}; Strain #006054)[23] mice were purchased from The Jackson Laboratory. $Rosa26^{LSL\text{-}Bcl2\text{-}IRES\text{-}GFP}$ mice[24] were provided by Dr. Hamid Kashkar (University of Cologne). $Rosa26^{INDIA}$ mice[25] were provided by Dr. Michel Nussenzweig (The Rockefeller University). B6.129S6-Stat5btm1Mam Stat5atm2Mam/Mmjax (STAT5a/b$^{fl/fl}$) mice[26] were provided by Dr. Hyun Park (National Cancer Institute). Brd4$^{fl/fl}$ mice[27] were provided by Dr. Dinah Singer (National Cancer Institute). C57BL/6-Tg (TcraTcrb)1100Mjb/J (OT-I)[28] and B6.Cg-Tg (TcraTcrb)425Cbn/J (OT-II)[29] mice expressing CD45.1 were provided by Drs. Alfred Singer and Paul Roche (National Cancer Institute). B6.129P2-B2mtm1Unc/DcrJ ($\beta2m^{-/-}$) mice[30] were provided by Dr. Alfred Singer (National Cancer Institute). $Rosa26^{LSL\text{-}Fucci2aR}$ mice[31] were provided by Dr. Ettore Appella (National Cancer Institute) and crossed with CMV^{Cre} mice to induce germline deletion of the loxP-STOP-loxP cassette. Following crossing to C57BL/6J mice, Cre-negative $Rosa26^{Fucci2aR}$ mice exhibiting ubiquitous Fucci2aR expression were subsequently intercrossed to homozygosity. Mice were maintained under specific pathogen-free conditions at NCI (Frederick and Bethesda) on a 12 h dark/light cycle. Male and female mice aged 6–18 weeks were used for all experiments.

2.2 Production, purification, and characterization of recombinant cytokines

A pcDNA3-based expression plasmid containing a human Fc tag (Addgene plasmid #141183) was modified to generate expression vectors encoding recombinant FLT3L or GM-CSF. The FLT3L construct encoded a murine immunoglobulin signal peptide[32], an Avi-tag, an N-terminal human Fc tag, and human FLT3L (Accession number AAA17999.1) amino acids 27 to 185. The GM-CSF construct encoded a murine immunoglobulin signal peptide[32], murine GM-CSF (Accession number Q14AD9) amino acids 18 to 141, a C-terminal human Fc tag, and an Avi-tag. Both plasmids are available upon request. Endotoxin-free plasmid DNA was purified using NucleoBond® Xtra Maxi EF (Takara #740424.50). Recombinant cytokines were produced by transient transfection of 293F cells and purified using Protein G Sepharose 4 Fast Flow (GE Healthcare) following the same recombinant protein expression and purification procedures previously described for antibodies[32,33]. Purified proteins were buffer exchanged into phosphate-buffered saline (PBS), sterile filtered, and analyzed by sodium dodecyl sulfate-polyacrylamide gel electrophoresis (SDS-PAGE) under reducing conditions (Figure S1A). Gels were imaged using a ChemiDoc Imaging System (Bio-Rad), and the inverted gel images were analyzed by densitometry in Fiji (ImageJ). Protein concentrations were determined using a NanoDrop One spectrophotometer (Thermo Fisher Scientific). Protein purity was calculated as the peak area of the major monomeric protein band divided by the total peak area of all detectable protein bands within the lane. Incompletely denatured higher molecular weight species were excluded from the purity calculation. Using this approach, FLT3L preparations exhibited purities ranging from 95% to 100%, whereas GM-CSF preparations exhibited a purity of 98%. Endotoxin levels in recombinant FLT3L and GM-CSF preparations were measured using the Pierce™ Chromogenic Endotoxin Quantification Kit (Invitrogen #A39552S) according to the manufacturer's instructions. Based on the cytokine concentrations used for iDC1 generation, endotoxin concentrations in iDC1 cultures were <0.0005 EU/mL across all tested preparations (Figure S1B,C).

2.3 Generation of BMDCs and induced $CD103^+$ cDC1 (iDC1)

Candidate fetal bovine serum (FBS) lots from multiple commercial vendors were evaluated by generating iDC1 cultures under identical conditions using the protocol described below. cDC1 yield, purity, and baseline expression of CD80, CD86, and CD40 were compared with a previously validated reference FBS lot. Representative FBS lot screening data are shown in Figure S2. As with other BMDC culture systems, FBS lot screening is recommended before initiating iDC1 cultures. Unless otherwise indicated, complete

culture medium consisted of Roswell Park Memorial Institute (RPMI) 1640 containing GlutaMAX or L-glutamine (Gibco #61870036 or Fisher Scientific #FB12999107) supplemented with 10% heat-inactivated FBS (Biofluids #200P-500, lot #814037 or GeminiBio #S11150, lot #K23233), 1× Penicillin-Streptomycin (Gibco #15070063), 1× 2-mercaptoethanol (Gibco #21985023), 25 mM 4-(2-hydroxyethyl)-1-piperazineethanesulfonic acid (HEPES) (Quality Biological #118-089-721 or Gibco #15630080), 2 mM additional GlutaMAX (Gibco #35050061), and 1 mM sodium pyruvate (Gibco #11360070). Where indicated, complete medium consisted of RPMI 1640, Dulbecco's Modified Eagle Medium (DMEM) containing high glucose and GlutaMAX (Gibco #10569044), or Iscove's Modified Dulbecco's Medium (IMDM) (Gibco #12440053), each supplemented with 10% heat-inactivated FBS, 1× Penicillin-Streptomycin, and 1× 2-mercaptoethanol. Media were additionally supplemented where indicated with 1× minimum essential medium (MEM) non-essential amino acids (Gibco #11140050) and 1× MEM amino acids (Gibco #11130051).

Femurs and tibiae were harvested from mice of the indicated genotypes, cut at both ends, and bone marrow was flushed with complete RPMI 1640 medium. Cells were passed through a 70 µm cell strainer, centrifuged for 7 min at 1,300 rpm, and subjected to red blood cell lysis using ammonium–chloride–potassium (ACK) lysis buffer (Quality Biological #118-156-101 or KD Medical #RGF-3015). Cells were subsequently washed and resuspended in complete RPMI 1640 medium.

GM-CSF-derived DCs (GM-Mac/DC), FLT3L-derived DC (FLT3L-DC), iCD103-DC and FLT3L/KitL-derived DC were generated as described previously[13,14,16,19,20], except that the optimized culture media described above and recombinant GM-CSF and FLT3L produced in-house were used. The initial bone marrow cell numbers were maintained as described in the original published protocols to preserve the established culture conditions. For direct comparison between BMDC methods, all cDC1 yields were calculated per 1×10^6 input bone marrow cells. All BMDC cultures were established in 100 mm × 15 mm non-tissue-culture-treated bacteriological Petri dishes (Falcon #351029 or Kord-Valmark #KORD-2910P) and maintained at 37 °C and 5% CO_2.

For GM-Mac/DC cultures, 2×10^6 bone marrow cells were cultured in 12 mL complete RPMI 1640 medium containing 20 ng/mL GM-CSF (in-house produced). On day 2, 10 mL fresh complete medium was added. On days 4, 6, and 8, 10 mL culture supernatant was collected, centrifuged, and cell pellets were resuspended in 10 mL fresh complete medium containing 20 ng/mL GM-CSF and returned to the original plates. Non-adherent cells were harvested on day 9.

For FLT3L-DC cultures, 15×10^6 cells were cultured in 12 mL complete RPMI 1640 medium containing 200 ng/mL FLT3L (in-house produced) for 9 days.

For KitL/FLT3L-DC cultures, 7.5×10^6 cells were cultured in 12 mL complete RPMI 1640 medium containing 200 ng/mL FLT3L (in-house produced) and 200 ng/mL recombinant murine KitL (PeproTech #250-03). On day 3, cells were harvested, centrifuged, resuspended in fresh medium containing 200 ng/mL FLT3L, and returned to the original plates. Cells were harvested on day 11.

For iCD103-DC cultures, 15×10^6 cells were cultured in 12 mL complete RPMI 1640 medium containing 200 ng/mL FLT3L and 2 ng/mL GM-CSF (both in-house produced). Non-adherent cells were harvested on day 9, counted, centrifuged, and 3×10^6 cells were replated in 12 mL complete RPMI 1640 medium containing 200 ng/mL FLT3L and 2 ng/mL GM-CSF. Cells were harvested on day 16.

For iDC1 cultures, 15×10^6 cells were cultured in complete RPMI 1640 medium containing 200 ng/mL FLT3L (in-house produced), 2 ng/mL GM-CSF (in-house produced), and 200 ng/mL KitL (PeproTech #250-03) for 9 days. Non-adherent cells were harvested on day 9, counted, centrifuged, and 3×10^6 cells were replated in 12 mL complete RPMI 1640 medium containing 200 ng/mL FLT3L and 2 ng/mL GM-CSF. The day 9 replating procedure was repeated on day 16, and non-adherent iDC1 were routinely harvested on day 23. For selected experiments, iDC1 cultures were established in 150 mm × 15 mm non-tissue-culture-treated bacteriological Petri dishes (Falcon #351058) in parallel, in which case culture volume and cell numbers were scaled proportionally to surface area (2.6-fold). For some experiments, iDC1 cultures were established using commercial recombinant cytokines in parallel with in-house produced cytokines. Commercial cytokines were used either at the same concentrations as the corresponding in-house cytokines (200 ng/mL FLT3L and 2 ng/mL GM-CSF) or at equimolar concentrations, as indicated for each cytokine: human FLT3L (Peprotech #300-19-100UG; 36.4 ng/mL), murine FLT3L (Peprotech #250-31L-100UG; 38.4 ng/mL), human Fc-tagged FLT3L (BioXcell #BE000098; 200 ng/mL), murine GM-CSF (Peprotech #315-03-100UG; 0.32 ng/mL).

2.4 Light microscopy

Light microscopy images were acquired directly from iDC1 culture dishes using an Axio Vert.A1 inverted microscope (Zeiss) equipped with 10× or 20× objectives and a Canon EOS Rebel SL3 camera.

2.5 Flow cytometry

For details about the antibodies used, see Supplementary Table S1. Flow cytometry data were acquired on a FACSymphony A5 (BD Biosciences) and analyzed using FlowJo version 10 (BD Biosciences). For live-cell staining, Fc receptors were blocked for 15 min on ice using anti-CD16/CD32 antibody (2.4G2, produced in-house). Cells were centrifuged for 3 min at 1300 rpm and stained with antibodies against surface antigens for 45 min at 4 °C, followed by three washes with fluorescence activated cell sorting (FACS) buffer (PBS containing 0.1% w/v bovine serum albumin (BSA) and 2 mM ethylenediaminetetraacetic acid (EDTA)). Where indicated, cells were

subsequently stained with APC-Fire750-conjugated streptavidin (BioLegend #405250; 1:320 dilution) for 10 min at 4 °C and washed three times. Cells were resuspended in FACS buffer containing 0.2 µg/mL propidium iodide (PI; Sigma-Aldrich #P4170) or 0.1 µg/mL DAPI (Sigma-Aldrich #D9542) before acquisition to exclude dead cells. For selected experiments, cells were incubated with 5 µM CellROX (Thermo Fisher Scientific #C10422) for 30 min at 37 °C, washed three times with PBS, and subsequently stained for surface markers.

For intracellular staining of 5-ethynyl-2′-deoxyuridine (EdU), active caspase-3 (aCasp3), and BRD4, cells were washed twice with PBS and stained with Zombie UV Fixable Viability Dye (BioLegend #423108; 1:500 dilution in PBS) for 30 min at 4 °C before Fc receptor blocking and surface staining.

For detection of EdU and aCasp3, cells were fixed and permeabilized using BD Cytofix/Cytoperm (BD #554714) for 30 min at 4 °C, followed by two washes with 1× Perm/Wash buffer (BD #554714). EdU incorporation was detected using Click-iT Plus EdU Alexa Fluor 488 Flow Cytometry Assay Kit (Thermo Fisher #C10632) according to the manufacturer's instructions. Cells were incubated with Click reaction mix for 30 min in the dark and washed twice with 1× Perm/Wash buffer. Where indicated, cells were subsequently stained with anti-aCasp3 antibody diluted in 1× Perm/Wash buffer for 45 min at 4 °C, washed twice with 1× Perm/Wash buffer, and resuspended in FACS buffer.

For detection of BRD4, cells were fixed with 2% paraformaldehyde (PFA; Electron Microscopy Sciences #15714-S) for 10 min at room temperature, washed twice with PBS, and permeabilized with pre-chilled methanol (Thermo Fisher #A412-1) on ice for 20 min. After two washes with FACS buffer, cells were incubated with rabbit anti-BRD4 antibody (Abcam #ab289886) for 30 min at room temperature followed by two washes with FACS buffer. Cells were then incubated with goat anti-rabbit Alexa Fluor 488 antibody (Abcam #ab150081; 1:1,000 dilution) for 30 min at room temperature, washed twice with FACS buffer, and resuspended in FACS buffer.

For detection of phosphorylated STAT5 (p-STAT5), cells were resuspended in sterile RPMI 1640 medium and rested for 30 min at 37 °C before stimulation with 2 ng/mL GM-CSF for 30 min at 37 °C. Cells were fixed with 1.6% PFA for 10 min at 37 °C, washed twice with HBSS (Gibco #14170-112) supplemented with 10% heat-inactivated FBS (Gemini #S11150, lot #K23233), and permeabilized with pre-chilled methanol (Thermo Fisher #A412-1) for 15 min on ice. After two washes with HBSS containing 10% FBS, cells were incubated with Fc block and p-STAT5 antibody for 30 min at room temperature followed by staining with antibodies against surface antigens for 20 min at room temperature. Cells were subsequently stained with allophycocyanin (APC)-Fire750-conjugated streptavidin (BioLegend #405250; 1:320 dilution) for 10 min at room temperature, washed twice with FACS buffer, and resuspended in FACS buffer.

2.6 Proteomics

Bcl-2-expressing iDC1 were generated from $Xcr1^{Cre}$ $Rosa26^{LSL\text{-}Bcl2\text{-}IRES\text{-}GFP}$ bone marrow to prevent apoptosis following GM-CSF withdrawal (Figure S3), harvested on day 23, and washed twice with complete RPMI 1640 medium. For each biological replicate, multiple plates each containing 3×10^6 iDC1 in 12 mL complete RPMI 1640 medium and either 200 ng/mL FLT3L alone or 200 ng/mL FLT3L plus 2 ng/mL GM-CSF were prepared and cultured for an additional 20 h at 37 °C and 5% CO_2. Non-adherent iDC1 were then harvested, pooled, washed twice with PBS, and cell pellets from seven biological replicates per condition were frozen prior to proteomic analysis.

Each cell pellet was lysed in 500 µL EasyPep Lysis Buffer (Thermo Fisher #A45735) supplemented with 1× phosphatase inhibitor (Thermo Fisher #A32957) and universal nuclease (Thermo Fisher #88700). Protein concentration was determined by bicinchoninic acid (BCA) assay and 150 µg protein from each sample was used for digestion. Two control and two GM-CSF-treated samples were digested twice to complete the tandem mass tag (TMT) pro plex and increase material available for phospho-peptide enrichment. Samples were adjusted to 150 µL total volume with lysis buffer and mixed with 50 µL digestion buffer containing 50 mM tris (2-carboxyethyl) phosphine (TCEP), 200 mM chloroacetamide, and 58 ng/µL trypsin/LysC in 75 mM HEPES (pH 8.0). Samples were incubated at 37 °C for 21 h and subsequently labeled with TMTpro 18-plex reagents (Thermo Fisher #A52045; lots 3214388 and 3214389) for 1 h at 25 °C. Excess TMTpro reagent was quenched with 5% hydroxylamine and 20% formic acid for 10 min, after which samples were combined. Peptides were cleaned using EasyPep Maxi columns (Thermo Fisher #A45734) according to the manufacturer's instructions and eluted in 3 mL elution buffer. Eluted peptides were divided into a 50 µL aliquot for global proteomic analysis and four 737 µL aliquots for phosphopeptide enrichment and subsequently dried.

Phospho-peptides were sequentially enriched using High-Select TiO_2 (Thermo Fisher #A32993) and High-Select Fe-NTA IMAC (Thermo Fisher #A32992) kits according to the manufacturer's instructions. Global and phospho-enriched peptide samples were resuspended in 0.1% formic acid and analyzed in duplicate using a Dionex U3000 rapid separation liquid chromatography instrument (RSLC) coupled to an Orbitrap Eclipse mass spectrometer (Thermo Fisher Scientific) equipped with an EasySpray ion source and field asymmetric ion mobility spectrometry (FAIMS) Duo interface. Peptides were separated by reverse-phase liquid chromatography and analyzed using Orbitrap-based data-dependent acquisition with TurboTMT quantification.

All mass spectrometry (MS) files were processed in Proteome Discoverer 2.4 using the Sequest search engine and searched against the UniProt mouse database. Searches were performed using full tryptic specificity with up to two missed cleavages, a precursor mass

tolerance of 10 ppm, and a fragment mass tolerance of 0.02 Da. Variable modifications included methionine oxidation (+15.995 Da) and serine, threonine, and tyrosine phosphorylation (+79.966 Da), whereas carbamidomethylation of cysteine (+57.021 Da) and TMTpro labeling of lysine residues and peptide N-termini (+304.207 Da) were specified as fixed modifications. Percolator was used for false discovery rate (FDR) analysis. Phosphosite localization was performed using IMP-ptmRS with a localization threshold of 90%. TMTpro reporter ions were quantified using the Reporter Ion Quantifier node and normalized on total peptide intensity for each channel.

Statistical analyses were performed in Proteome Discoverer 2.4 using $\log_2$-transformed median intensities and analysis of variance (ANOVA)-based p-value calculation. Proteomic and phospho-proteomic differential abundance analyses were considered exploratory, and proteins and phospho-peptides meeting prespecified thresholds of absolute $\log_2$ fold change ($\log_2$FC) > 0.6 and nominal $p < 0.05$ were included in downstream analyses. p values were not adjusted for multiple testing. Proteins or peptides detected in at least two replicates of one condition and absent from all replicates of the comparison condition were assigned adjusted $\log_2$FC and p-values to permit inclusion in downstream analyses. TMTpro channel assignments are provided in Data S1.

GM-CSF-regulated differentially abundant proteins were analyzed using Ingenuity Pathway Analysis, and enriched transcription factor target signatures were analyzed using the Database for Annotation, Visualization, and Integrated Discovery (DAVID; https://davidbioinformatics.nih.gov/). Ingenuity Pathway Analysis was considered exploratory and reports nominal pathway significance as -log(p value) together with activation z scores (Data S2). DAVID transcription factor enrichment results report Fisher's exact p values together with Benjamini, Bonferroni, and FDR corrections (Data S3).

2.7 FACS sorting and RNA sequencing analysis

BMDCs were generated as described above and either left unstimulated or stimulated overnight (~16 h) with 10 µg/mL Poly(I:C) (InvivoGen #tlrl-pic). Non-adherent BMDCs were harvested, stained for flow cytometry as described above, and directly sorted into Trizol LS Reagent (Thermo Fisher #10296010) using a FACSymphony S6 (BD Biosciences).

Three to four biological replicates of each population were sorted after excluding DAPI$^+$ cells. GM-Mac/DC cultures were gated as CD11c$^+$ CD11b$^+$ I-A/I-E^{low} CD64$^+$ CD115$^+$ macrophages. FLT3L, iCD103-DC and iDC1 cultures were gated as CD64$^-$ CD11c$^+$ CD45R/B220$^-$ CD103$^+$ CD172a$^-$ Xcr1$^+$ CD24$^+$ cDC1. Additional populations sorted from FLT3L-DC cultures included CD64$^-$ CD11c$^+$ CD45R/B220$^-$ CD103$^-$ CD172a$^-$ Xcr1$^+$ CD24$^+$ cDC1, CD64$^-$ CD11c$^+$ CD45R/B220$^-$CD103$^-$ CD172a$^+$ Xcr1$^-$ CD24^{low} cDC2, and CD64$^+$CD172a$^+$ macrophages.

For tissue DC and macrophage isolation, spleens and lungs from C57BL/6 mice were injected with digestion buffer containing HBSS (Gibco #14170-112), 4 mM calcium chloride (Quality Biological #351-130-721), 1 mM magnesium chloride (Quality Biological #351-033-721), and 10% heat-inactivated FBS (Biofluids #200P-500, lot #814037). Spleens were digested with 1 mg/mL Collagenase D (Millipore Sigma #11088858001) and 0.1 mg/mL DNase I (Millipore Sigma #11284932001), whereas lungs were digested with 0.2 mg/mL Collagenase IV (Millipore Sigma #C4-22-1g) and 0.1 mg/mL DNase I. Tissues were minced and incubated at 37 °C for 25 min (spleen) or 90 min (lung). Subsequently, 10 mM EDTA (Invitrogen #15575-038) was added for 5 min and tissues were passed through a 70 µm cell strainer.

Single-cell suspensions were centrifuged for 7 min at 1300 rpm and resuspended in high-density medium consisting of three parts HBSS and one part OptiPrep (Serumwerk Bernburg AG #1893). Suspensions were overlaid with low-density medium consisting of one part OptiPrep and 4.2 parts FACS buffer, followed by a final HBSS overlay. Density gradients were centrifuged for 15 min at 1,500 rpm and 4 °C without brake. Low-density cells enriched for DCs and macrophages were collected from the interphase, washed with FACS buffer, stained for flow cytometry as described above, and directly sorted into TRIzol LS Reagent using a FACSymphony S6.

Lineage markers included CD19, Ter-119, and NK1.1. Three biological replicates of each population were sorted after exclusion of DAPI$^+$ cells. Splenic populations included Lineage$^-$ CD45R/B220$^-$ I-A/I-E^{high} CD11c^{high} CD3ε$^-$ CD45$^+$ CD11b$^-$ Xcr1$^+$ cDC1, Lineage$^-$ CD45R/B220$^-$I-A/I-E^{high} CD11c^{high} CD3ε$^-$ CD45$^+$ CD11b$^+$ Xcr1$^-$ cDC2, and Lineage$^-$ CD45R/B220$^-$ CD11c^{low} I-A/I-E^{low} F4/80$^+$ CD11b$^+$ CD3ε$^-$ CD45$^+$ red pulp macrophages. Lung alveolar macrophages were gated as Lineage$^-$ CD45$^+$ SiglecF$^+$ CD11c$^+$ cells.

Total RNA was extracted according to the manufacturer's instructions for Trizol-LS. 1 µL Pellet Paint (Novagen #69049) was added to the aqueous phase prior to RNA precipitation with isopropanol to facilitate precipitation and pellet visualization. Extracted RNA was further purified with the Nucleospin RNA XS kit (Takara Bio #740902.50) according to the manufacturer's instructions. Subsequently, 100 pg total RNA was processed using the SMARTer Ultra Low Input RNA Kit (Takara) to generate cDNA libraries. Sequencing libraries were then prepared using the Nextera XT DNA Sample Preparation Kit (Illumina). Sixty samples were pooled and sequenced on a NovaSeq X Plus 1.5B instrument using paired-end sequencing.

Raw fastq files were aligned and quantified using the NF Core RNA seq pipeline (https://zenodo.org/records/20072251). Quantified reads were analyzed by using tximport[34] to import reads and annotations, and counts normalized using edgeR[35,36] using trimmed mean of the M-values. Limma-voom[37] and variancePartition[38,39] were used to perform linear modeling with mixed effects to identify differentially expressed genes between conditions. The day 23 iDC1 samples without stimulation were used as a baseline for comparison against all other conditions, with batch as a random effect. Gene set enrichment analysis (GSEA) was performed using clusterProfiler[40] on the log fold changes generated by the variancePartition mixed-effects model, with gene sets obtained using

msigdbr (https://CRAN.R-project.org/package=msigdbr). Differential expression results are reported with adjusted *p* values (Data S4 and Data S5). GSEA results are reported with normalized enrichment scores (NES), nominal *p* values, and adjusted *q* values (Data S6 and Data S7). ImmGen database was accessed using celldex and compared against limma-voom transformed data using SingleR[41]. SingleR applies labels from a reference dataset to a query dataset by selecting interesting features using differential expression between labels in the reference and using nearest neighbor indices in rank space. Spearman rank correlation is used to specify which reference label is applied to each query sample, with the label with the highest score being applied to the query.

2.8 iDC1 stimulation

Non-adherent day 23 iDC1 were harvested, counted, washed once with sterile PBS, and resuspended in complete RPMI 1640 medium. Subsequently, 2×10^5 iDC1 were plated in 200 µL complete RPMI 1640 medium in non-tissue-culture-treated 96-well round-bottom plates and stimulated with 100 ng/mL lipopolysaccharide (LPS) (Sigma #L2630), 10 µg/mL poly(I:C) (InvivoGen #tlrl-pic), 1 µM CpG-ODN 1826 (InvivoGen #tlrl-1826), combined poly(I:C) plus CpG-ODN 1826, or left untreated for 21-22 h at 37 °C and 5% CO_2. Cell pellets were analyzed for co-stimulatory marker expression by flow cytometry. Culture supernatants were analyzed using the Proteome Profiler Mouse XL Cytokine Array Kit (R&D Systems #ARY028) according to the manufacturer's instructions. Array membranes were developed using SuperSignal West Pico PLUS Chemiluminescent Substrate (Thermo Fisher #34577), and chemiluminescent signals were imaged using a UVP ChemStudio system (Analytik Jena). Images were analyzed using ImageJ. Relative protein expression levels were quantified by measuring spot mean gray values, which were averaged across duplicate spots and two independent experiments. Spots with average mean gray values greater than 20 were considered positive.

2.9 Preparation of heat-killed Listeria monocytogenes expressing OVA

All agar plates and liquid media were supplemented with 50 µg/mL erythromycin (Sigma #E5389). Frozen *Listeria monocytogenes* expressing ovalbumin (OVA) (LM-OVA)[42] were streaked onto brain heart infusion (BHI) agar plates and incubated overnight at 37 °C. A single colony was inoculated into 4 mL BHI medium and cultured overnight at 37 °C and 225 rpm. The following day, 150 mL pre-warmed BHI medium was inoculated to an OD_{600} of approximately 0.1 and cultured at 37 °C and 225 rpm until reaching an OD_{600} of approximately 0.5-1.5. Cultures were centrifuged for 20 min at 4000 rpm, and bacterial pellets were washed twice with 50 mL sterile PBS by centrifugation for 10 min at 4,000 rpm. LM-OVA were resuspended to an estimated concentration of 1×10^{11} CFU/mL based on the approximation that an OD_{600} of 0.1 corresponds to 2×10^8 CFU/mL[43]. LM-OVA stocks were heat-inactivated by incubation for 1 h at 70 °C (heat-killed *Listeria monocytogenes* expressing OVA (HKLM-OVA)) and stored at -80 °C. Complete inactivation was confirmed by absence of colony growth on BHI agar plates.

2.10 *In vitro* antigen cross-presentation assay

Non-adherent day 23 wild-type (WT) and *Irf8*$^{+32-/-}$ iDC1 were harvested, counted, and resuspended in complete RPMI 1640 medium. B cells were purified from C57BL/6 spleens following red blood cell lysis with ACK lysis buffer using Mouse CD43 Microbeads (Miltenyi Biotec #130-049-801) and LS columns (Miltenyi Biotec #130-042-401) according to the manufacturer's instructions. B cell preparations routinely exceeded 98% purity as assessed by flow cytometry. Purified B cells were counted and resuspended in complete RPMI 1640 medium. $CD8^+$ T cells were purified from spleens and lymph nodes of $CD45.1^+$ OT-I mice using the Mouse $CD8a^+$ T cell Isolation Kit (Miltenyi Biotec #130-104-075) and LS columns according to the manufacturer's instructions. Purified $CD8^+$ T cells were washed with sterile PBS and labeled with 5 µM CellTrace Violet (CTV; Invitrogen #C34557) for 20 min at 37 °C according to the manufacturer's instructions. Cells were subsequently counted, centrifuged, and resuspended in complete RPMI 1640 medium. For cross-presentation assays, 2.5×10^4 CTV-labeled OT-I T cells were cultured with 1×10^4 iDC1 or 1×10^4 B cells in the presence of either 10^8 HKLM-OVA[42], 10 µg/mL soluble OVA (Sigma #A5503), 1 µg/mL SIINFEKL peptide ($OVA_{257-264}$; Life Technologies), or no stimulation. After 4 days at 37 °C, proliferation of CTV^{low} $CD44^+$ $CD8\alpha^+$ $CD45.1^+$ $V\alpha2^+$ OT-I T cells was analyzed by flow cytometry as percentages and total cell numbers.

2.11 *In vivo* antigen cross-presentation assay

WT and *Irf8*$^{+32-/-}$ mice received intravenous transfer of 1×10^6 each of CTV-labeled OT-I and OT-II T cells. OT-I T cells were purified as described above, whereas OT-II T cells were purified with the Mouse $CD4^+$ T cell Isolation Kit (Miltenyi Biotec #130-104-454). CTV-labeling was performed as described above. A subset of *Irf8*$^{+32-/-}$ mice additionally received 1×10^7 iDC1 intravenously. One day later, mice were injected intravenously with 2×10^7 irradiated OVA-pulsed $\beta2m^{-/-}$ splenocytes or vehicle alone. $\beta2m^{-/-}$ splenocytes were resuspended in RPMI 1640, irradiated with 1500 rads, incubated with 10 mg/mL OVA (Sigma #A5503) in RPMI 1640 for 10 min at 37 °C, and washed three times prior to injection[44]. Four days later, spleens were harvested, total viable splenocytes were counted, and OT-I and OT-II expansion and proliferation were analyzed by flow cytometry.

2.12 Statistical analysis

Statistical analyses were performed using GraphPad Prism software (version 10). Data were assessed for normality using the Anderson-Darling, D'Agostino-Pearson, Shapiro-Wilk, and Kolmogorov-Smirnov tests where applicable. Unpaired two-tailed Student's *t*-tests were used for normally distributed data or when sample size was insufficient for normality testing. Statistical tests used are

indicated in the figures and figure legends. For statistical analyses performed using GraphPad Prism, no adjustments were made for multiple comparisons because the analyses were limited to pre-specified pairwise comparisons. Statistical methods for RNA-seq, proteomic, phospho-proteomic, and downstream enrichment analyses are described in the corresponding Methods sections.

3. Results and Discussion

3.1 Culture media type and composition regulate cDC1 production

We first assessed whether culture conditions influence cDC1 production using previously described iCD103-DC cultures generated with FLT3L and low-dose GM-CSF that strongly enrich for CD103$^+$ cDC1[19]. RPMI 1640 generated significantly more cDC1 than IMDM and DMEM (Figure S4A,B,C), indicating that basal media composition strongly influences cDC1 differentiation efficiency. Compared with RPMI 1640, IMDM and DMEM contain higher concentrations of amino acids. Consistently, supplementation of RPMI 1640 with excess essential and non-essential amino acids significantly reduced cDC1 generation relative to control RPMI 1640 cultures (Figure S4D,E,F), suggesting that elevated amino acid availability suppresses efficient cDC1 differentiation. These findings suggest that cDC1 differentiation is highly sensitive to extracellular metabolic conditions. Elevated amino acid availability may alter nutrient-sensing and metabolic pathways required for efficient cDC1 differentiation, including pathways linked to mTOR signaling[45] and cellular biosynthetic activity.

In contrast, supplementation of RPMI 1640 with HEPES, sodium pyruvate, and the stable dipeptide *L*-glutamine substitute GlutaMAX (this supplement mixture is abbreviated as HSpG) significantly increased cDC1 production (Figure S4A,B,C), consistent with metabolic support and buffering capacity promoting cDC1 expansion and/or survival. Based on these findings, RPMI 1640 supplemented with HSpG was used for subsequent experiments. Together, these findings identify extracellular metabolic conditions as an important determinant of efficient cDC1 generation and establish RPMI 1640 supplemented with HSpG as an optimized basal medium for subsequent iDC1 cultures.

3.2 iDC1 cultures produce large numbers of +32 kb *Irf8* enhancer-dependent cDC1 of high purity

We next established a distinct BMDC culture system incorporating the defined RPMI 1640 medium supplemented with HSpG together with FLT3L, low-dose GM-CSF, and KitL during the first 9 days of culture, followed by serial replating with FLT3L and GM-CSF every 7 days (termed iDC1; Figure 1a). For comparison, previously described iCD103-DC cultures generated with FLT3L and low-dose GM-CSF that effectively enrich for CD103$^+$ cDC1[19] were analyzed in parallel using the same medium. Flow cytometric analysis at days 16, 23, and 30 showed that iDC1 cultures exhibited higher cDC1 purity than iCD103-DC cultures at days 16 and 23, while by day 30 iCD103-DC cultures approached the similarly high purity achieved by iDC1. At all time points, however, iDC1 cultures generated markedly greater cDC1 yields than iCD103-DC cultures (Figure 1b,c). Overall cDC1 purity increased from ~60% in day 16 iCD103-DC cultures to ~97% in day 23 iDC1 cultures (Figure 1b), with total cDC1 yields peaking at day 23 (Figure 1c), representing an approximately 75-fold increase relative to the original iCD103-DC method using recombinant cytokines[19]. Day 23 therefore provided the optimal balance between maximal cDC1 yield and very high purity, whereas extending cultures to day 30 did not provide a further increase in cDC1 yield. Day 23 was therefore selected for all subsequent experiments. Comparison of iCD103-DC and iDC1 cultures at day 16 isolates the effect of KitL, as both protocols have identical culture duration and replating history. Extension of both protocols to day 23 with an additional replating step demonstrates that the marked increase in cDC1 yield achieved by iDC1 cannot be explained by prolonged culture or serial replating alone.

iDC1 cultures established in 100 mm dishes could be scaled to 150 mm dishes with only a modest reduction in yield and purity, while remaining highly efficient for cDC1 generation (Figure S4G,H,I). To assess protocol robustness across serum lots, multiple commercially available FBS lots were evaluated using the iDC1 protocol. Several independent FBS vendors and lots supported efficient iDC1 generation, demonstrating reproducibility across serum sources, although FBS lot testing is recommended prior to selecting a particular lot for iDC1 generation (Figure S2).

We additionally assessed reproducibility across independently produced cytokine preparations. High-purity cDC1 generation was achieved across independent FLT3L lots, demonstrating lot-to-lot reproducibility of the in-house FLT3L preparations (Figure S1D). We next tested whether iDC1 could be generated using commercially available recombinant FLT3L and GM-CSF rather than the in-house cytokines used throughout this study. At the same mass concentrations used for the in-house cytokines, commercial recombinant cytokines supported efficient iDC1 generation, with comparable or slightly higher cDC1 purity (Figure S1E,F). cDC1 yields were also comparable or trended higher with commercial human FLT3L and Fc-tagged human FLT3L, whereas yields were reduced with murine FLT3L (Figure S1G). Thus, efficient iDC1 generation is not dependent on the in-house cytokine preparations.

At concentrations equimolar to the in-house Fc-fusion proteins, cDC1 purity was maintained with commercial human FLT3L and Fc-tagged human FLT3L but was significantly reduced with murine FLT3L, whereas cDC1 yields were substantially reduced across all equimolar conditions (Figure S1E,F,G). Notably, when Fc-tagged human FLT3L was maintained at an equimolar concentration, increasing commercial murine GM-CSF from its equimolar concentration (0.32 ng/mL) to 2 ng/mL restored cDC1 yield (Figure S1G). These findings suggest greater apparent bioactivity of the in-house Fc-tagged GM-CSF compared with monomeric recombinant

GM-CSF under these culture conditions. The dimeric structure of the Fc-tagged in-house GM-CSF may contribute to this difference, although other differences between the recombinant preparations cannot be excluded. cDC1 generated with commercial recombinant cytokines generally expressed Xcr1 at levels comparable to those generated with the in-house cytokines, with slightly lower expression observed only when using 200 ng/mL commercial human FLT3L and 2 ng/mL commercial mouse GM-CSF (Figure S1H,I).

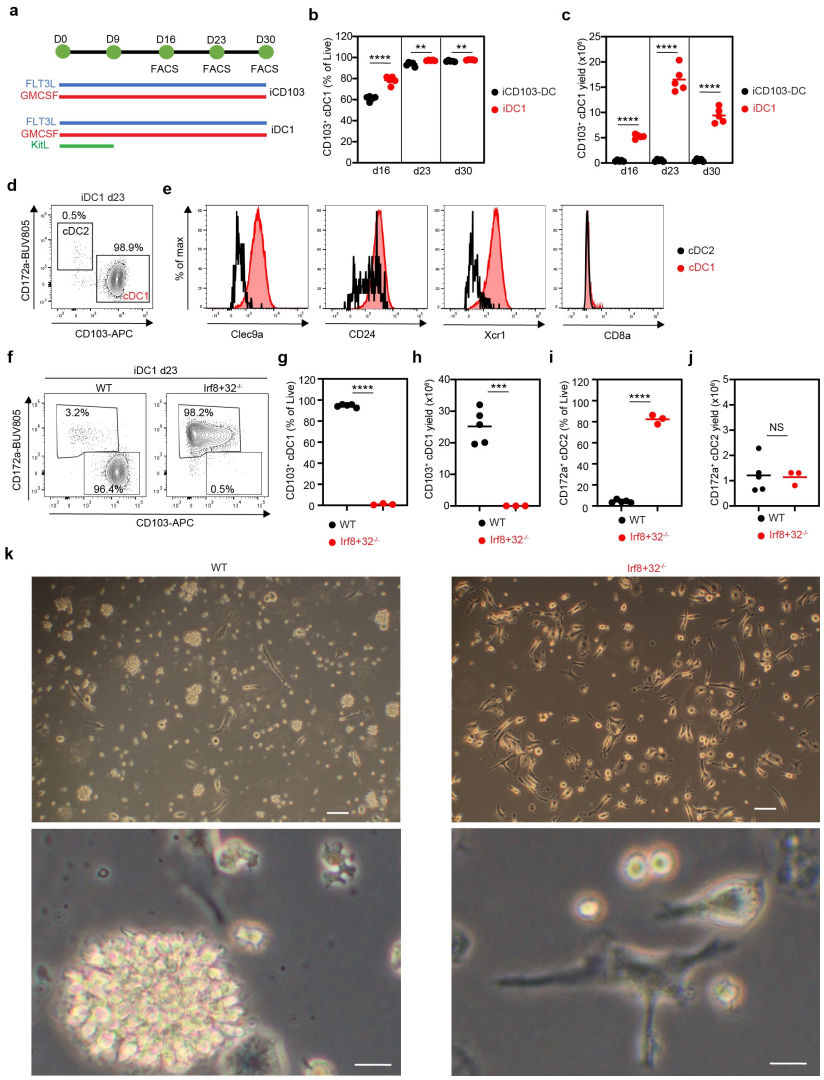


Figure 1. Efficient generation of pure CD103$^+$ cDC1 in iDC1 cultures requires the +32 kb *Irf8* enhancer. (a-e) Bone marrow cells were cultured with FLT3L and GM-CSF (iCD103-DC) or with FLT3L, GM-CSF, and KitL (iDC1), followed by serial replating with FLT3L and GM-CSF every 7 days. Cells were analyzed by flow cytometry at the indicated time points. (a-c) One representative experiment including all three time points is shown. Similar results were obtained in four additional independent experiments, including one experiment containing day 23 and day 30 analyses and three additional experiments containing day 16 analyses. (a) Experimental scheme; (b) Frequencies and (c) total numbers of CD103$^+$ cDC1 at the indicated time points; (d, e) One representative experiment of three independent experiments, each including four to five biological replicates, is shown; (d) Representative contour plot of CD103 versus CD172a expression among CD11c$^+$ CD45R/B220$^-$ CD64$^-$ cDC from day 23 iDC1 cultures; (e) Expression of indicated markers in cDC1 and cDC2 from day 23 iDC1 cultures; (f-k) iDC1 cultures were generated from WT or *Irf8*$^{+32-/-}$ bone marrow and analyzed on day 23; (f-j) One representative of two independent experiments, each including five biological replicates per genotype, is shown. (f) Representative contour plots showing cDC1 and cDC2 populations among CD11c$^+$ CD45R/B220$^-$ CD64$^-$ cDC; (g) Frequency and (h) total number of cDC1; (i) Frequency and (j) total number of cDC2; (k) Representative micrographs from one of six independent experiments (scale bars, 100 μm (top) and 20 μm (bottom)). ** $p < 0.01$, *** $p < 0.001$, **** $p < 0.0001$, NS = not statistically significant (unpaired two-tailed Student's *t*-test). cDC1: conventional type 1 dendritic cells; iDC1: induced cDC1; FLT3L: fms-related tyrosine kinase 3 ligand; KitL: kit ligand; GM-CSF: granulocyte-macrophage colony-stimulating factor; WT: wild-type; APC: antigen-presenting cell; FACS: fluorescence activated cell sorting; cDC2: conventional type 2 dendritic cells.

CD103$^+$ CD172a$^-$ iDC1 expressed canonical cDC1 markers including CD24, Clec9a, and Xcr1, but not CD8α, whereas these markers were absent or expressed at lower levels in the trace CD103$^-$ CD172a$^+$ cDC2 population within the same cultures (Figure 1d,e), consistent with the previously described iCD103-DC phenotype[19].

To determine lineage identity, iDC1 cultures were established from control and *Irf8*$^{+32-/-}$ bone marrow. CD103$^+$ CD172a$^-$ cDC1 were absent in *Irf8*$^{+32-/-}$ cultures compared with WT controls (Figure 1f,g,h), whereas remaining cells were predominantly cDC2 (Figure 1f,g,h,i) with total numbers comparable to WT controls (Figure 1j). iDC1 cultures formed floating aggregates and single cells with dendritic morphology (Figure 1k), similar to iCD103-DC cultures[19], whereas *Irf8*$^{+32-/-}$ cultures lacked floating clusters. Together, these findings establish iDC1 cultures as a scalable system for high-yield, high-purity generation of +32 kb *Irf8* enhancer-dependent cDC1.

3.3 Comparison of iDC1 to other BMDCs, tissue DCs and macrophages

We next compared the overall cellular composition of different BMDC systems at their established endpoint culture times using a common flow cytometry gating strategy (Figure S5A). GM-CSF-derived cultures (GM-Mac/DC) and FLT3L-derived cultures (FLT3L-DC) were analyzed on day 9, FLT3L/KitL cultures on day 11, iCD103-DC cultures on day 16, and iDC1 cultures on day 23. GM-Mac/DC cultures contained predominantly CD172a$^+$ CD64$^+$ cells (86%) expressing high levels of CD11b and F4/80 and low levels of I-A/I-E (Figure 2a and Figure S5), consistent with a macrophage phenotype[12]. The remaining cells could not be clearly separated from macrophages. Together, these findings confirm that GM-CSF cultures predominantly generate macrophage-like populations rather than cDC1[12,19].

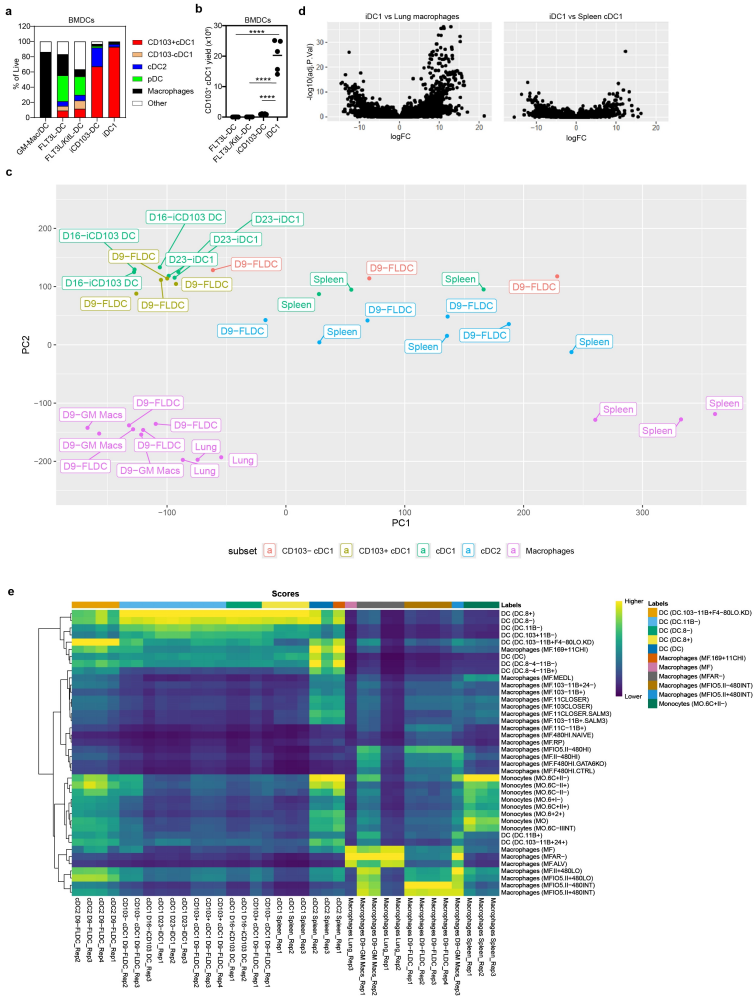


Figure 2. iDC1 cultures generate homogeneous CD103$^+$ cDC1 with phenotypic and transcriptional features of the cDC1 lineage. (a, b) iDC1 were compared with other BMDC culture systems by flow cytometry. One representative of three independent experiments, each including 4-5 biological replicates, is shown; (a) Cellular composition; (b) Total numbers of CD103$^+$ cDC1 generated per 1 × 10^6 bone marrow input cells; (c, d) RNA-seq analysis of DC and macrophage populations purified from indicated BMDC cultures and tissues; (c) Principal component analysis; (d) Volcano plots showing differentially expressed genes in iDC1 compared with lung macrophages (left) and splenic cDC1 (right); (e) Heatmap showing SingleR comparison of the indicated BMDC and tissue DC and macrophage populations (columns) with the ImmGen reference atlas. Rows show the ImmGen reference populations identified as the most similar across the analyzed samples, with higher SingleR scores indicating greater transcriptional similarity to the corresponding reference population. **** $p < 0.0001$ (unpaired two-tailed Student's *t*-test). iDC1: induced cDC1; cDC1: conventional type 1 dendritic cells; BMDC: bone marrow-derived DC; DC: dendritic cell; cDC2: conventional type 2 dendritic cells; FLT3L: fms-related tyrosine kinase 3 ligand; KitL: kit ligand; FLDC: feedback linearizing dynamic controller; WT: wild-type.

FLT3L-DC cultures were highly heterogeneous, comprising 15.2% cDC1, 6.2% cDC2, and 34.0% pDCs (Figure 2a). cDC1 could be further subdivided into CD103$^+$ and CD103$^-$ subsets (9.1% and 6.1%, respectively), both expressing CD24 and Xcr1 (Figure 2a and Figure S5A). FLT3L-DC also contained 27.8% CD172a$^+$ CD64$^+$ macrophage-like cells expressing F4/80 and CD11b with low I-A/I-E, as well as 16.8% cells that did not fall within cDC1, cDC2, or macrophage gates (Figure 2a and Figure S5A). FLT3L/KitL cultures showed a broadly similar composition but with increased cDC1 frequencies and reduced pDCs and macrophage populations (Figure 2a and Figure S5A). Together, these findings demonstrate that FLT3L-based cultures generate a broad spectrum of DC and macrophage populations and therefore provide a heterogeneous system suited to study DC subset development and lineage relationships, but not selective cDC1 generation.

iCD103-DC cultures contained 67.2% CD103$^+$ cDC1 and 24.7% cDC2, with minimal pDCs (2.1%), macrophages (2.7%), and non-DC populations (3.3%), confirming enrichment for CD103$^+$ cDC1 relative to FLT3L-based systems[19] but retaining a residual cDC2 fraction.

In contrast, iDC1 cultures contained 92.8% CD103$^+$ cDC1, did not generate appreciable CD103$^-$ cDC1 populations, and included < 3.5% cDC2, pDCs, macrophages, or non-DCs, respectively (Figure 2a and Figure S5A), demonstrating a marked increase in homogeneity relative to all other BMDC systems tested. CD103$^+$ cDC1 from iDC1 cultures lacked F4/80 expression, expressed low CD11b, and exhibited higher I-A/I-E levels compared with CD172a$^+$ CD64$^+$ cells from GM-Mac/DC and FLT3L-DC cultures (Figure S5B), consistent with a cDC1 phenotype. A direct side-by-side comparison demonstrated that iDC1 expressed equivalent or slightly higher levels of XCR1 than FLT3L-derived cDC1 (Figure S6), a receptor that mediates XCL1-dependent interactions with NK cells and CD8$^+$ T cells[46,47]. In addition, iDC1 cultures produced substantially higher total numbers of CD103$^+$ cDC1 than all other BMDC methods tested when normalized to 1×10^6 input bone marrow cells for direct comparison (Figure 2b). Together, these findings demonstrate that iDC1 cultures markedly improve both cDC1 purity and scalability relative to existing BMDC systems. Thus, whereas FLT3L-based cultures provide heterogeneous systems for studying multiple DC subsets, iCD103-DC and iDC1 cultures progressively increase selective enrichment of cells with cDC1 characteristics, with iDC1 achieving substantially greater purity and scalability.

To further define the transcriptional relationship between iDC1, other BMDCs, tissue DCs, and macrophages, we sorted CD103$^+$ cDC1 (from iDC1, iCD103-DC, and FLT3L-DC cultures), CD103$^-$ cDC1 (from FLT3L-DC cultures), cDC2 (from FLT3L-DC cultures and spleen), CD64$^+$ cells (from GM-Mac/DC and FLT3L-DC cultures), and tissue cDC1 and macrophages (from spleen and lung) by flow cytometry, followed by RNA-seq. Principal component analysis showed that CD64$^+$ cells from GM-Mac/DC and FLT3L-DC cultures localized in close proximity to lung alveolar macrophages and were clearly separated from iDC1 and cDC populations (Figure 2c). In contrast, iDC1 localized within the broader cDC1 region of the PCA plot together with CD103$^+$ cDC1 generated in iCD103-DC and FLT3L-DC cultures, as well as CD103□ FLT3L-derived and splenic cDC1, whereas cDC2 populations occupied a distinct region of the PCA plot within the broader cDC distribution (Figure 2c). Splenic red pulp macrophages occupied a distinct region separate from both cDC populations and lung alveolar macrophages (Figure 2c). Consistent with the PCA, differential expression analysis identified fewer transcriptional differences between iDC1 and splenic cDC1 than between iDC1 and lung alveolar macrophages (Figure 2d). Differentially expressed genes between iDC1 and splenic cDC1 are provided in Data S5. GSEA of this comparison showed that the transcriptional differences involved specific biological processes, including antigen processing and presentation, immune signaling, protein translation and oxidative phosphorylation, as well as cell-cycle-associated pathways (Data S7). These differences may reflect distinct cytokine exposure and other environmental conditions between cultured iDC1 and splenic cDC1. Although iDC1 and splenic cDC1 are not transcriptionally identical, these findings support the conclusion that iDC1 are transcriptionally aligned with the cDC1 lineage rather than macrophages.

We next compared the BMDC populations from our dataset with the ImmGen reference atlas using SingleR-based analysis to independently assess their transcriptional identity. Primary splenic cDC1, splenic cDC2, splenic macrophages, and lung macrophages from our RNA-seq dataset were included as additional primary comparator populations. The ImmGen reference contains 830 microarray samples representing 253 finely resolved immune cell subtypes. cDC1 populations from iDC1, iCD103-DC, and FLT3L-DC cultures showed highest similarity to a restricted group of cDC1-associated ImmGen reference populations, including DC.8$^+$, DC.8$^-$, DC.11B$^-$, and DC.103$^+$11B$^-$ (Figure 2e). These BMDC cDC1 populations showed ImmGen reference profiles similar to primary splenic cDC1 and clustered adjacent to them, whereas FLT3L-derived cDC2 formed a distinct group. Primary splenic cDC1 and cDC2 clustered together within the broader cDC-associated portion of the analysis. Similarly, cultured, lung, and splenic macrophages showed preferential similarity to macrophage-associated ImmGen reference populations while retaining differences associated with culture or tissue origin. Together, these findings provide independent reference-based support for the cDC1 transcriptional identity of iDC1, while also revealing differences between BMDC and primary tissue populations.

3.4 iDC1 respond to innate stimulation and cross-present cell-associated antigen

To evaluate whether iDC1 respond to innate stimuli, particularly via TLR3, a cDC1 signature gene[48], we stimulated iDC1 with TLR ligands and analyzed expression of co-stimulatory molecules by flow cytometry. iDC1 responded to LPS, poly(I:C), and CpG ODN1826 (CpG) stimulation by upregulating CD80, CD86, and CD40, whereas co-stimulation with poly(I:C) and CpG further increased CD80 and CD40 expression (Figure 3a,b). In contrast, CD103 expression remained largely unchanged across conditions (Figure 3a).

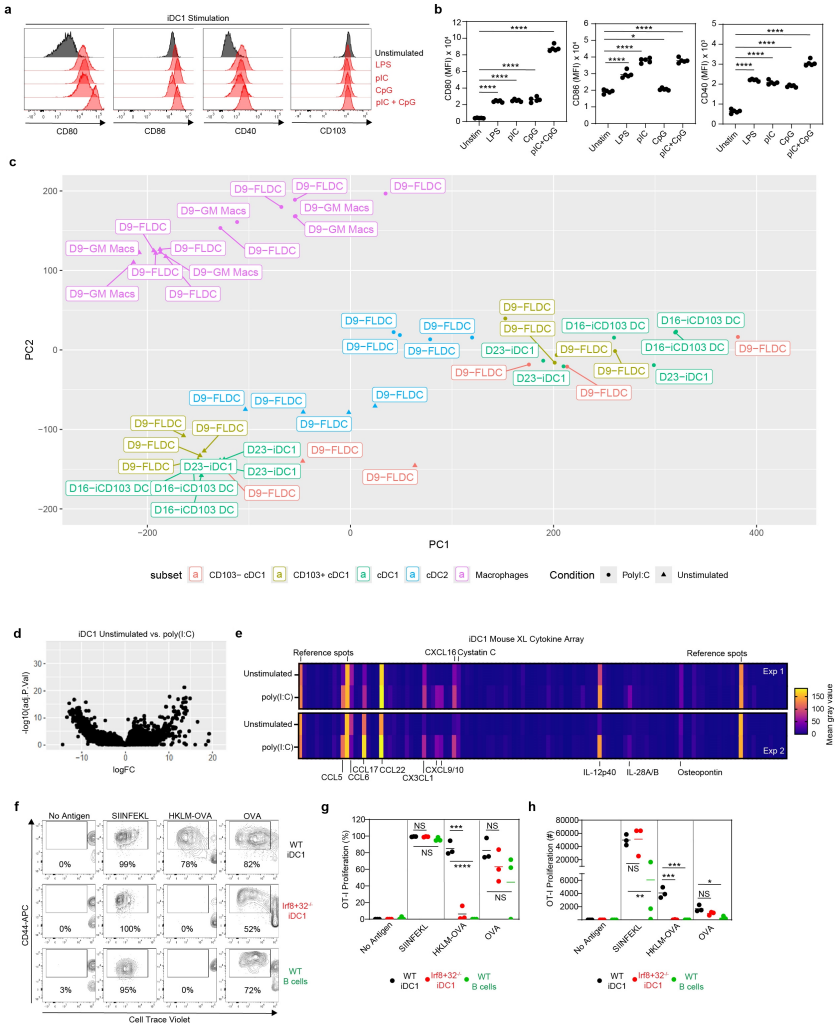


Figure 3. iDC1 respond to innate stimulation and exhibit functional properties of cDC1. (a, b) iDC1 were left unstimulated or stimulated overnight with LPS, poly(I:C) (pIC), CpG ODN1826 (CpG), or combined pIC and CpG. One of two independent experiments, each including 5 biological replicates, is shown. (a) Representative half-offset histograms showing CD80, CD86, CD40, and CD103 expression under unstimulated (black) and indicated stimulated conditions (red); (b) Quantification of MFI; (c, d) RNA-seq analysis of DC and macrophage populations purified from indicated BMDC cultures that were either unstimulated or stimulated overnight with poly(I:C); (c) Principal component analysis; (d) Volcano plot showing differentially expressed genes between unstimulated and poly(I:C)-stimulated iDC1; (e) Supernatants from unstimulated or poly(I:C)-stimulated iDC1 cultures were analyzed using a Mouse XL cytokine array. Heatmaps MGV for 111 targets from two independent experiments. Data represent the average of duplicate spots within each experiment. Targets detected above threshold (MGV > 20) in either condition are annotated; (f-h) CTV-labelled $CD8^+$ OT-I T cells were co-cultured with equal numbers of WT iDC1, *Irf8*$^{+32-/-}$ iDC1, or B cells and were left unstimulated or stimulated with SIINFEKL peptide, cell-associated OVA (heat-killed *Listeria monocytogenes* expressing OVA; HKLM-OVA), or soluble OVA for 4 days; (f) Representative contour plots showing CTV dilution and CD44 expression of $CD8^+$ $CD45.1^+$ $V\alpha2^+$ OT-I cells under the indicated conditions; (g, h) Quantification of proliferated (CTV^{low} $CD44^+$) OT-I cells as (g) percentages and (h) total cell numbers. Data are combined from three independent experiments. Each data point represents the mean of three technical replicates from one independent experiment; (b, g, h) * $p < 0.05$, ** $p < 0.01$, *** $p < 0.001$, **** $p < 0.0001$; NS, not statistically significant (two-tailed unpaired Student's *t*-test). iDC1: induced cDC1; cDC1: conventional type 1 dendritic cells; MFI: mean fluorescence intensities; BMDC: bone marrow-derived DC; MGV: mean gray values; CTV: cell trace violet; WT: wild-type; HKLM-OVA: heat-killed *Listeria monocytogenes* expressing OVA; IL: interleukin.

To define the transcriptional response of iDC1 to poly(I:C) stimulation and compare it with other BMDC populations, we performed RNA-seq. Principal component analysis (PCA) showed that macrophages occupied a distinct region of the PCA plot, separate from cDC populations (Figure 3c). Following poly(I:C) stimulation, $CD103^+$ cDC1 from iDC1, iCD103-DC, and FLT3L-DC cultures exhibited a more pronounced transcriptional shift compared with cDC2 and macrophages (Figure 3c). This enhanced transcriptional responsiveness is consistent with the specialized sensitivity of cDC1 to nucleic acid sensing pathways mediated by TLR3[2]. In iDC1, 3,324 genes were differentially expressed following poly(I:C) stimulation (Figure 3d and Data S4). GSEA revealed that the top upregulated pathways were associated with interferon signaling, antiviral responses, inflammatory cytokine signaling, and innate immune activation, whereas downregulated pathways were enriched for cell-cycle, DNA replication, and proliferation-associated programs (Data S6). Poly(I:C)

stimulation therefore appears to shift iDC1 from a proliferative steady-state program toward an inflammatory state characterized by enhanced interferon signaling, innate activation, and cytokine-associated transcriptional responses.

To assess the functional consequences of poly(I:C) stimulation at the protein level, we profiled supernatants from unstimulated and poly(I:C)-stimulated iDC1 cultures using a Mouse XL cytokine array. iDC1 increased secretion of IL-12p40 in response to stimulation (Figure 3e), a hallmark cytokine produced by activated cDC1[2-4]. Stimulated iDC1 also secreted chemokines including CCL5 (RANTES), CCL17 (TARC), CCL22 (MDC), CX3CL1 (Fractalkine), CXCL9 (MIG), CXCL10 (IP-10), and CXCL16, whereas secretion of CCL6 (C10) was reduced following poly(I:C) stimulation (Figure 3e). Several induced chemokines, including CXCL9, CXCL10, CCL5, and CX3CL1, are associated with recruitment and activation of cytotoxic lymphocytes and Th1-associated immune responses, consistent with established cDC1 functions[2-4]. Poly(I:C)-stimulated iDC1 also secreted IL-28A/B, whereas Cystatin C and Osteopontin were detected under both unstimulated and stimulated conditions (Figure 3e), further supporting the inflammatory response induced by poly(I:C).

We next compared WT iDC1, *Irf8*$^{+32-/-}$ iDC1 (comprising cDC2 generated under identical conditions; Figure 1f), and B cells for their capacity to cross-present cell-associated and soluble OVA to OT-I T cells. No OT-I proliferation was observed in the absence of antigen, while all antigen-presenting cell (APC) types induced robust OT-I proliferation in response to SIINFEKL peptide (Figure 3f,g,h). Strikingly, WT iDC1, but not *Irf8*$^{+32-/-}$ iDC1 or B cells, efficiently cross-presented cell-associated OVA (HKLM-OVA). Soluble OVA induced OT-I proliferation in the presence of all three APC populations, with no significant differences in the percentage of proliferated cells. However, the total number of proliferated OT-I cells was greater with WT iDC1 than with B cells, whereas the response induced by *Irf8*$^{+32-/-}$ iDC1 was not significantly different from that induced by WT iDC1 (Figure 3f,g,h). Together, these data demonstrate that iDC1 respond robustly to innate stimulation and exhibit hallmark functional characteristics of the cDC1 lineage, including inflammatory cytokine production and efficient cross-presentation of cell-associated antigen.

3.5 *In vivo* function of iDC1

To assess whether iDC1 can cross-present cell-associated antigen *in vivo*, we transferred CTV-labelled OT-I and OT-II T cells into WT or *Irf8*$^{+32-/-}$ mice. A subset of *Irf8*$^{+32-/-}$ mice additionally received iDC1 intravenously. One day later, mice were intravenously administered OVA-pulsed β2m$^{-/-}$ splenocytes as a source of cell-associated antigen or vehicle alone. Four days later, OT-I and OT-II T cell proliferation was analyzed by flow cytometry (Figure 4a).

Minimal OT-I T cell expansion and proliferation occurred in the absence of antigen, whereas *Irf8*$^{+32-/-}$ mice exhibited impaired OT-I expansion and proliferation in response to OVA-pulsed β2m$^{-/-}$ splenocytes compared with WT mice (Figure 4b,c,d,e), consistent with the established requirement for cDC1 in cross-presentation[2,6]. Responses following iDC1 transfer were heterogeneous, with two of four recipients exhibiting OT-I responses comparable to those observed in WT mice, whereas the remaining recipients showed little or no rescue (Figure 4b,c,d,e). In contrast, OT-II T cell proliferation was comparable between WT and *Irf8*$^{+32-/-}$ mice and was not substantially altered by iDC1 transfer (Figure 4f,g,h,i). Together, these findings provide evidence that transferred iDC1 can cross-present cell-associated antigen and promote OT-I responses *in vivo*, although responses varied between recipients under these experimental conditions.

3.6 GM-CSF and KitL regulate distinct stages of cDC1 generation in iDC1 cultures

To define how KitL and GM-CSF contribute to cDC1 generation during the 23-day iDC1 culture period, we compared five conditions: (1) iDC1 control, (2) no GM-CSF from day 9 to day 23, (3) no GM-CSF throughout the culture period, (4) no GM-CSF from day 0 to day 9, and (5) no KitL (extended iCD103-DC control; Figure 5a). iDC1 control cultures generated the highest purity of CD103$^+$ cDC1, whereas purity was most reduced when GM-CSF was absent throughout the culture (condition 3) and was also significantly decreased when GM-CSF was removed from day 9 to day 23 (condition 2; Figure 5b). iDC1 control cultures also produced the highest total numbers of CD103$^+$ cDC1, whereas all cytokine perturbation conditions markedly reduced cDC1 yields (Figure 5c). Notably, removal of GM-CSF during the early culture phase (condition 4) or omission of KitL (condition 5) substantially reduced total cDC1 numbers without markedly affecting cDC1 purity, indicating that early KitL and GM-CSF are required to achieve maximal cDC1 yield. Together, these results indicate that KitL and GM-CSF cooperate during the early phase of culture, whereas GM-CSF remains necessary during the later phase to maintain optimal cDC1 yield and purity, suggesting that GM-CSF directly regulates the maintenance of differentiated cDC1.

Early human studies likewise established *in vitro* generation of CD141$^+$/BDCA3$^+$ cDC1-like cells from CD34$^+$ hematopoietic progenitors using multi-step cytokine differentiation protocols[49,50]. Although these studies differed in their cytokine combinations, collectively employing FLT3L together with additional cytokines including SCF, GM-CSF, IL-4, IL-3/IL-6, and/or thrombopoietin (TPO)[49-51], they demonstrated the feasibility of cytokine-driven cDC1 differentiation in humans. More recent studies have further improved the efficiency of human cDC1 generation through additional culture refinements, highlighting the continued evolution of *in vitro* cDC1 differentiation strategies toward translational applications[52-54]. Our findings extend these observations by showing that, in the mouse system, transient KitL together with FLT3L and low-dose GM-CSF is sufficient for highly efficient iDC1 generation. These comparisons suggest that efficient cDC1 generation depends not only on cytokine composition but also on culture design, including the timing and duration of cytokine exposure.

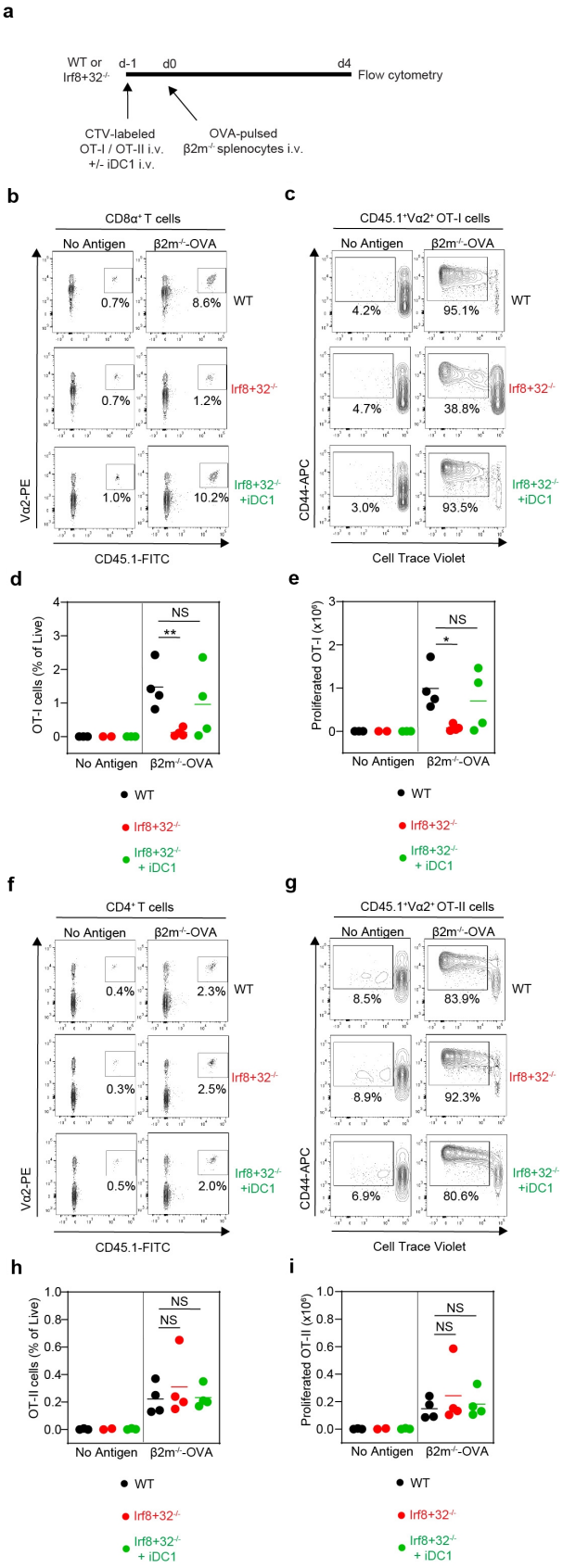


Figure 4. Transferred iDC1 can support cross-presentation of cell-associated antigen *in vivo*. WT or *Irf8*$^{+32-/-}$ mice received CTV-labeled OT-I and OT-II T cells, and a subset of *Irf8*$^{+32-/-}$ mice additionally received iDC1 intravenously. One day later, mice received OVA-pulsed β2m$^{-/-}$ splenocytes or vehicle alone intravenously and were analyzed four days

later. (a) Experimental scheme; (b, c) Representative contour plots showing (b) CD45.1 and Vα2 expression among CD8⁺ T cells, with gates identifying OT-I cells, and (c) CTV and CD44 expression among OT-I cells, with gates identifying proliferated activated OT-I cells; (d, e) Quantification of (d) OT-I cells as a percentage of live cells and (e) total proliferated activated OT-I cells per spleen; (f-i) Corresponding analysis of OT-II cells. Representative contour plots show (f) CD45.1 and Vα2 expression among CD4⁺ T cells, with gates identifying OT-II cells, and (g) CTV and CD44 expression among OT-II cells, with gates identifying proliferated activated OT-II cells; (h, i) Quantification of (h) OT-II cells as a percentage of live cells and (i) total proliferated activated OT-II cells per spleen; (d, e, h, i) Data are combined from two independent experiments, each including 1-3 mice per experimental condition, with four mice total per antigen-treated condition and 2-3 mice total for no-antigen controls. * $p < 0.05$, ** $p < 0.01$; NS, not statistically significant (two-tailed unpaired Student's *t*-test). iDC1: induced cDC1; CTV: cell trace violet; WT: wild-type; OVA: ovalbumin.

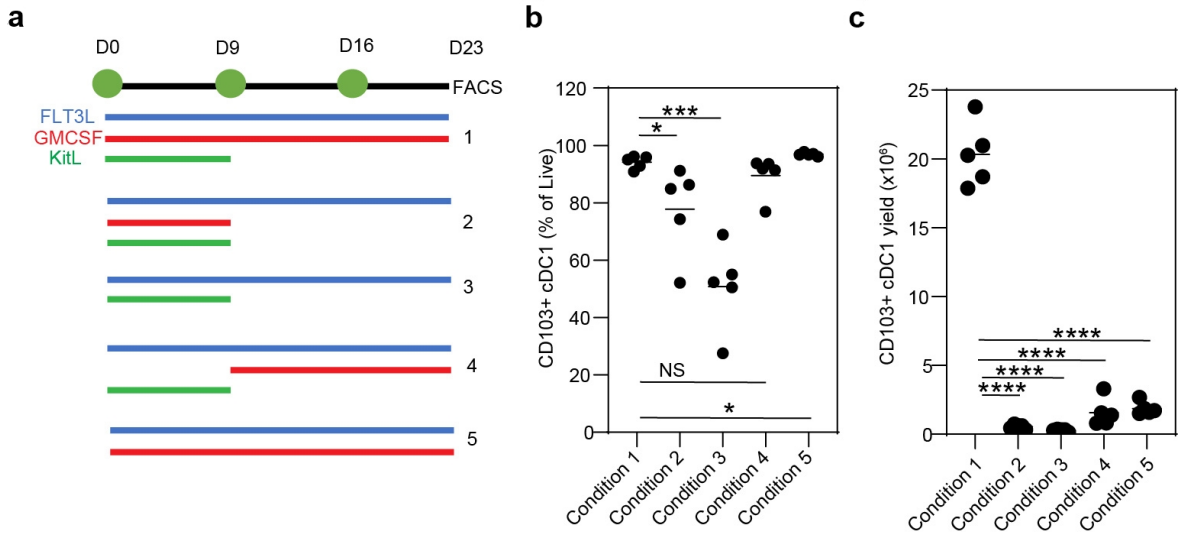


Figure 5. GM-CSF and KitL regulate distinct stages of cDC1 generation in iDC1 cultures. iDC1 and indicated variants were generated and analyzed by flow cytometry. One representative of two independent experiments, each including five biological replicates, is shown. (a) Overview of conditions tested; (b) Frequency of CD103⁺ cDC1 among live cells; (c) Total numbers of CD103⁺ cDC1 generated per 1 × 10^6 input bone marrow cells. * $p < 0.05$, *** $p < 0.001$, **** $p < 0.0001$; NS, not statistically significant (two-tailed unpaired Student's *t*-test). GM-CSF: granulocyte-macrophage colony-stimulating factor; cDC1: conventional type 1 dendritic cells; iDC1: induced cDC1; FACS: fluorescence activated cell sorting; FLT3L: fms-related tyrosine kinase 3 ligand; KitL: kit ligand.

3.7 Proteomic analysis identifies GM-CSF-regulated pathways in iDC1

We next sought to define the GM-CSF-regulated pathways and biological processes sustaining the late phase of efficient cDC1 generation in iDC1 cultures. Because GM-CSF withdrawal could reduce cDC1 viability and therefore compromise proteomic resolution, we first tested whether Bcl-2 expression preserves cDC1 survival under these conditions. iDC1 cultures were therefore generated from $Xcr1^{Cre}$ controls and $Xcr1^{Cre}$ $Rosa26^{LSL\text{-}Bcl2\text{-}IRES\text{-}GFP}$ bone marrow, resulting in Bcl-2 and GFP reporter expression in cDC1, followed by ~21 h culture with FLT3L alone or FLT3L plus GM-CSF (Figure S3A). Bcl-2 expression, indicated by GFP reporter expression, did not affect CD103⁺ cDC1 generation on day 23 and only modestly affected survival on day 24 in the continued presence of GM-CSF (Figure S3B,C,D,E). In contrast, Bcl-2 markedly enhanced cDC1 survival following GM-CSF withdrawal, restoring viability to levels comparable with controls maintained in GM-CSF (Figure S3B,C,D,E).

To identify GM-CSF-regulated pathways independently of acute effects on cell viability, iDC1 cultures generated from $Xcr1^{Cre}$ $Rosa26^{LSL\text{-}Bcl2\text{-}IRES\text{-}GFP}$ bone marrow were cultured for 20 h with FLT3L alone or FLT3L plus GM-CSF prior to proteomic analysis (Figure 6a). Using the prespecified exploratory thresholds of absolute $\log_2FC > 0.6$ and nominal $p < 0.05$, 45 proteins were increased and 12 proteins were decreased following GM-CSF treatment (Figure 6b). In addition, 268 phosphorylation events were increased and 45 were decreased using the same thresholds (Figure 6c). Ingenuity pathway analysis identified prominent regulation of RHO GTPase signaling, cytoskeletal organization, membrane trafficking, and endocytosis pathways in both datasets (Figure 6d,e and Data S2). These pathways are notable because cytoskeletal remodeling and membrane trafficking are central to DC migration, antigen uptake, and cross-presentation, processes previously linked to GM-CSF signaling[55-58]. Apoptotic execution, oxidative stress-, and metabolism-associated pathways were also represented in both the global and phospho-proteomic datasets, whereas phospho-proteomic analysis more prominently identified pathways associated with cell-cycle progression, chromosomal replication, and transcriptional regulation (Figure 6d,e and Data S2). Additional phospho-proteomic pathways included RNA Polymerase II transcription, DNA methylation and transcriptional repression signaling, and pathways linked to vesicular trafficking and cytoskeletal remodeling, suggesting that GM-CSF maintains a broadly active transcriptional and biosynthetic state in differentiated iDC1.

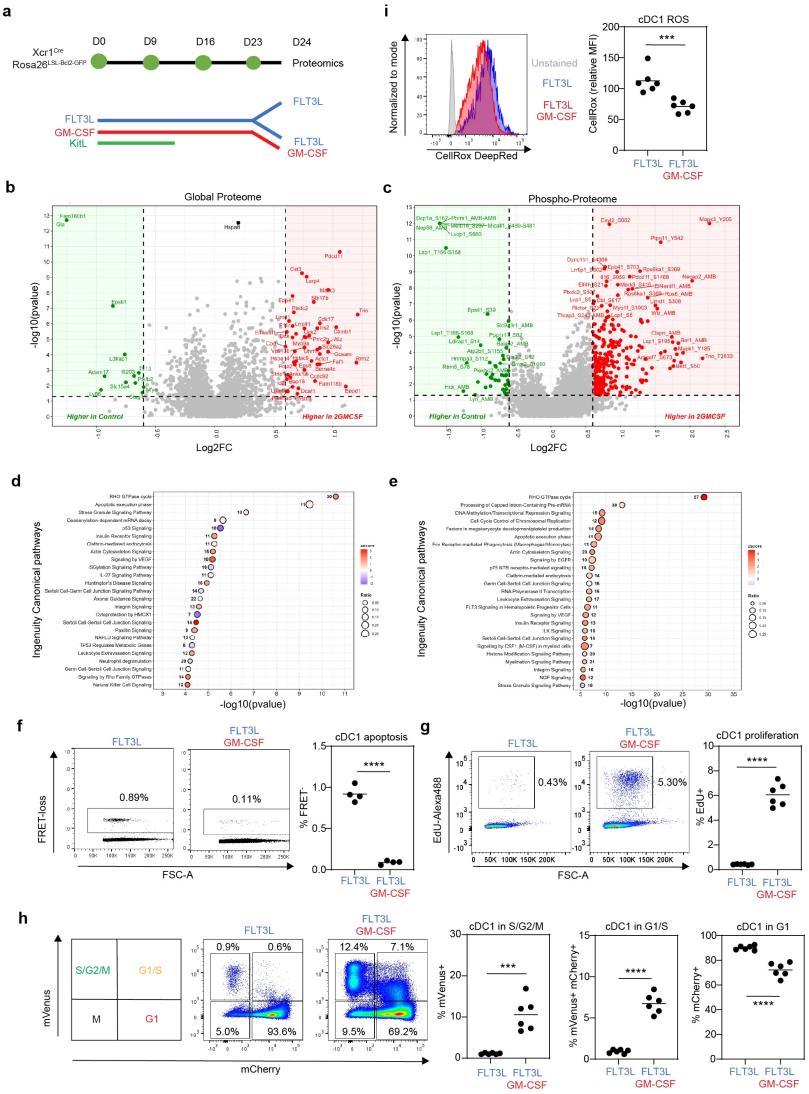


Figure 6. Proteomic and phospho-proteomic analyses identify GM-CSF-regulated signaling and biological programs in iDC1. iDC1 cultures were generated from the indicated genotypes for 23 days and subsequently cultured for an additional 20-21 h with FLT3L alone or FLT3L plus GM-CSF. (a-e) Proteomic and phospho-proteomic analyses. Xcr1^{Cre} Rosa26$^{LSL\text{-}Bcl2\text{-}IRES\text{-}GFP}$ bone marrow was used to prevent apoptosis following GM-CSF withdrawal (Figure S3). (a) Experimental scheme; (b, c) Volcano plots showing GM-CSF-regulated (b) proteins and (c) phosphorylation events; (d, e) Ingenuity pathway analysis of GM-CSF-regulated (d) proteins and (e) phosphorylation events. The top 25 pathways are shown; (f) Analysis of cDC1 apoptosis using Rosa26^{INDIA} bone marrow. Representative dot plots on the left show the percentage of FRET$^-$ early apoptotic cells, with quantification shown on the right. One representative of two independent experiments, each including 3-4 biological replicates, is shown; (g) Analysis of EdU incorporation to identify cDC1 in S phase of the cell cycle. Representative contour plots on the left show FSC and EdU incorporation, with quantification of EdU$^+$ cDC1 shown on the right. Data are combined from two independent experiments, each including three biological replicates; (h) Rosa26^{Fucci2aR} bone marrow was used to assess cell-cycle stages. Representative contour plots on the left show percentages of cDC1 in G1, G1/S, and S/G2/M phases, with quantification shown on the right. Data are combined from two independent experiments, each including three biological replicates; (i) iDC1 were stained with CellROX FarRed dye to assess ROS. Histograms on the left show CellROX staining of iDC1 cultured with FLT3L alone (blue), FLT3L plus GM-CSF (red), or unstained control (gray). CellROX MFI is quantified on the right. Data are combined from two independent experiments, each including three biological replicates. (b-e) Proteomic, phosphoproteomic, and IPA analyses were exploratory; nominal *p* values were not adjusted for multiple testing; (f-i) *** $p < 0.001$, **** $p < 0.0001$; NS, not significant (two-tailed unpaired Student's *t*-test). FLT3L: fms-related tyrosine kinase 3 ligand; KitL: kit ligand; GM-CSF: granulocyte-macrophage colony-stimulating factor; iDC1: induced cDC1; cDC1: conventional type 1 dendritic cells; MFI: mean fluorescence intensity; FSC: forward scatter; ROS: reactive oxygen species; EdU: 5-ethynyl-2'-deoxyuridine; IPA: ingenuity pathway analysis.

Notably, phosphorylation of Mapk3/Erk1 at the activating Y205 site represented one of the strongest GM-CSF-regulated phospho-events (Figure 6c), together with signaling changes consistent with engagement of MAPK-, PI3K/AKT-, mTOR-, and STAT5-associated pathways downstream of GM-CSF signaling[59] (Data S2). Additional regulated phosphosites included Ptpn11/SHP2 Y542 and Rps6ka1 S369, further supporting activation of canonical GM-CSF-associated MAPK signaling networks. Previous transcriptomic studies linked GM-CSF-responsive transcriptional programs to cDC1 survival and proliferation programs[60]. Our proteomic and phospho-proteomic analyses extend these findings by identifying coordinated regulation of signaling, cytoskeletal, membrane

trafficking, oxidative stress, and transcriptional programs associated with maintenance of differentiated cDC1. Together, these data suggest that GM-CSF supports a proliferative, transcriptionally active, and survival-permissive state associated with extensive cytoskeletal and membrane trafficking programs in differentiated iDC1.

3.8 GM-CSF promotes survival and proliferation of differentiated cDC1

To functionally validate the proteomic findings, we generated iDC1 cultures from Rosa26^{INDIA} mice, which sensitively report active caspase-3 through loss of fluorescence resonance energy transfer (FRET)[25]. GM-CSF significantly suppressed FRET loss in cDC1 (Figure 6f), whereas this effect was less apparent in cDC2 within the same cultures, although low cDC2 numbers limited this analysis (Figure S7A). We next quantified cells in S phase of the cell cycle by pulsing iDC1 cultures with EdU for 2 h followed by flow cytometric detection of EdU incorporation into DNA. GM-CSF significantly increased the percentage of cDC1 in S phase, whereas the effect was less pronounced in cDC2 (Figure 6g and Figure S7B). As an independent approach to assess cell-cycle progression, we generated iDC1 cultures from Rosa26^{Fucci2aR} mice[31], which distinguish G1, G1/S, and S/G2/M phases through mCherry and mVenus expression. GM-CSF markedly increased the percentages of cDC1 in G1/S and S/G2/M phases while decreasing the proportion of cells in G1 (Figure 6h). These changes were less pronounced or absent in cDC2 (Figure S7C). We also evaluated production of reactive oxygen species (ROS) in live cDC1 by staining with the cell-permeable dye CellROX FarRed. GM-CSF significantly reduced ROS production (Figure 6i), consistent with a role for GM-CSF in maintaining redox homeostasis and limiting apoptosis. Together, these experiments validate the major biological programs identified by the proteomic analyses and demonstrate that GM-CSF suppresses apoptosis, limits oxidative stress, and promotes cDC1 cell-cycle progression, thereby contributing mechanistically to the preferential outgrowth and sustained maintenance of cDC1 during the later stages of iDC1 culture.

3.9 STAT5- and BRD4-associated regulatory programs contribute to efficient iDC1 generation

Transcription factor target enrichment analysis implicated STAT5-, IRF8/BATF-, MYC-, and BRD4-associated regulatory programs among GM-CSF-responsive proteins (Data S3). STAT5 is a canonical downstream mediator of GM-CSF signaling[58], whereas MYC-associated programs have previously been linked to GM-CSF-dependent cDC1 proliferation and survival[60]. BRD4 regulates transcriptional elongation and MYC-associated transcriptional programs linked to highly active cellular states[27,61]. We therefore investigated whether STAT5 and BRD4 contribute to efficient cDC1 generation in iDC1 cultures.

To assess the role of STAT5, iDC1 cultures were generated from Xcr1^{Cre} Stat5a/b$^{fl/fl}$ bone marrow and corresponding controls. Functional loss of STAT5 signaling in Xcr1^{Cre} Stat5a/b$^{fl/fl}$ cDC1 was confirmed by flow cytometric analysis of phosphorylated STAT5 (p-STAT5) following GM-CSF stimulation, which showed markedly reduced p-STAT5 induction relative to stimulated controls (Figure S8A). Although STAT5-deficient iDC1 cultures retained comparably high cDC1 frequencies within the gated cDC compartment (Figure 7a), overall cDC1 purity was modestly but significantly reduced relative to control iDC1 cultures (Figure 7b), accompanied by small increases in cDC2 and macrophage populations (Figure 7c). More importantly, total CD103$^+$ cDC1 yields were markedly reduced in Xcr1^{Cre} Stat5a/b$^{fl/fl}$ iDC1 cultures compared with WT controls (Figure 7d), indicating that STAT5 contributes to efficient cDC1 generation in iDC1 cultures. Residual STAT5-deficient cDC1 also exhibited significantly reduced CD11c and CD103 expression, consistent with the representative contour plots (Figure 7a and Figure S8B) and the corresponding quantitative analyses (Figure S8C,D), in agreement with previous studies linking GM-CSF signaling to regulation of the CD103$^+$ cDC1 phenotype[55]. To determine whether STAT5 contributes to GM-CSF-mediated regulation of cDC1 proliferation and survival, day 23 iDC1 were cultured with FLT3L plus GM-CSF for 21 h prior to analysis of EdU incorporation and aCasp3. Xcr1^{Cre} Stat5a/b$^{fl/fl}$ cDC1 exhibited significantly reduced proportions of EdU$^+$ cells in S phase of the cell cycle (Figure 7e,f), accompanied by significantly increased frequencies of aCasp3$^+$ apoptotic cells (Figure 7g,h). Together, these findings support a role for STAT5 downstream of GM-CSF signaling in promoting cDC1 proliferation and survival, extending previous observations that conditional STAT5 deletion reduces CD103$^+$ DC populations in non-lymphoid tissues[62,63].

Because the role of BRD4 in cDC1 biology remains poorly defined, we next assessed its contribution to iDC1 generation by establishing iDC1 cultures from Xcr1^{Cre} Brd4$^{fl/fl}$ bone marrow. BRD4 expression by control cDC1 was efficiently ablated in Xcr1^{Cre} Brd4$^{fl/fl}$ cDC1 (Figure S8E). Brd4 deficiency caused pronounced CD11c downregulation and significant CD103 upregulation (Figure 7i and Figure S8F). These findings suggest that BRD4 regulates multiple aspects of the differentiated cDC1 phenotype. Additionally, CD103$^+$ cDC1 purity was significantly reduced (Figure 7i,j), mainly due to increases in cDC2, macrophages, and cells not falling within any of the gates (Figure 7k). Most importantly, BRD4 deficiency almost completely abrogated cDC1 generation in iDC1 cultures (Figure 7l). To further define the functional role of BRD4 during iDC1 generation, BRD4-deficient iDC1 were cultured with FLT3L and GM-CSF, pulsed with EdU, and analyzed for proliferation and apoptosis. BRD4 deficiency resulted in significantly reduced EdU incorporation together with increased aCasp3 staining compared with corresponding controls (Figure 7m,n,o,p), indicating that BRD4 contributes to efficient iDC1 generation by promoting proliferation while limiting apoptosis.

The current study has several limitations. The iDC1 protocol requires a prolonged culture period, sustained supplementation with recombinant cytokines, and FBS lot screening. Although our data identify functional roles for STAT5- and BRD4-associated regulatory programs during efficient iDC1 generation, the downstream transcriptional targets and their direct relationship to the canonical

Irf8/Batf3 cDC1 transcriptional network remain to be defined. Future optimization of culture duration, cytokine requirements, and serum-free or xeno-free culture conditions may facilitate the development of simplified cDC1-generation protocols for translational applications.

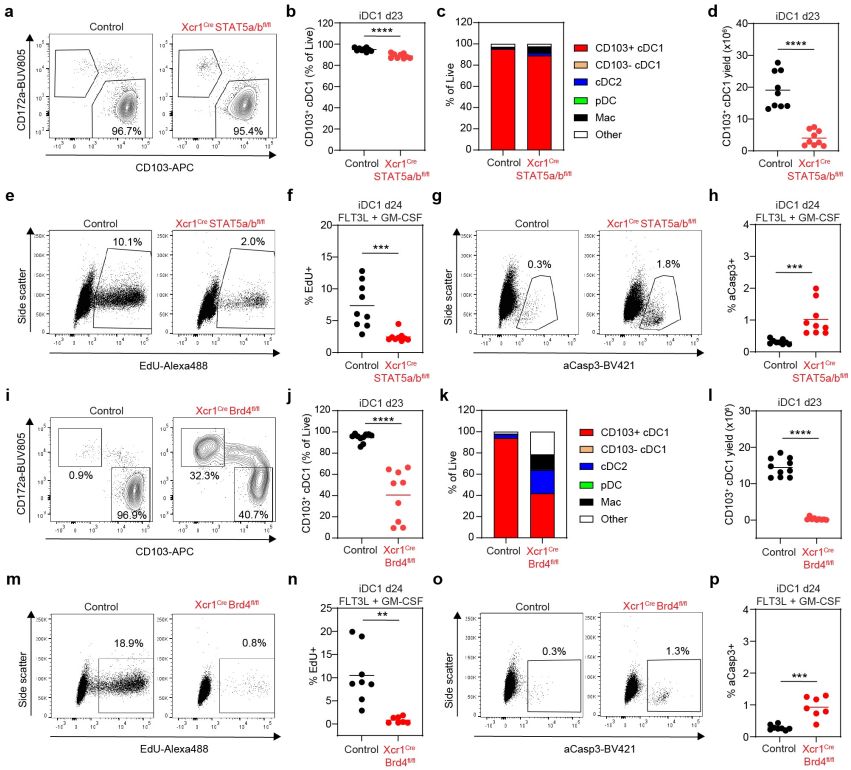


Figure 7. STAT5- and BRD4-associated regulatory programs contribute to efficient iDC1 generation. iDC1 cultures were generated from the indicated genotypes for 23 days and analyzed by flow cytometry on day 23 or cultured with FLT3L plus GM-CSF for 20-21 h, pulsed with EdU during the final 2 h of culture, and analyzed by flow cytometry on day 24. (a-h) Analysis of (a-d) day 23 or (e-h) day 24 STAT5-deficient iDC1 cultures. Control mice consisted of either C57BL/6J or Xcr1^{WT} Stat5a/b$^{fl/fl}$ mice. Results are combined from two independent experiments, each including 4-5 biological replicates per genotype. (a) Representative contour plots showing CD103 and CD172a expression and percentages of cDC1 among CD11c^{+} CD45R/B220^{-} CD64^{-} cDC; (b) Quantification of CD103^{+} cDC1 purity; (c) Average composition of iDC1 cultures across replicates and experiments; (d) Total numbers of CD103^{+} cDC1 generated per 1 × 10^{6} input bone marrow cells; (e) Representative dot plots showing EdU staining, side scatter, and percentages of EdU^{+} cDC1; (f) Quantification of EdU^{+} cDC1; (g) Representative dot plots showing aCasp3 staining, side scatter, and percentages of aCasp3^{+} cDC1; (h) Quantification of aCasp3^{+} cDC1; (i-p) Analysis of day 23 (i-l) or day 24 (m-p) BRD4-deficient iDC1 cultures. Control mice consisted of either Xcr1^{Cre} Brd4^{WT} or Xcr1^{WT} Brd4$^{fl/fl}$ mice; (i-l) Day 23 results are combined from four independent experiments, each including 1-4 biological replicates per genotype; (m-p) Day 24 results are combined from two independent experiments, each including 3-4 biological replicates per genotype; (i) Representative contour plots showing CD103 and CD172a expression and percentages of cDC1 and cDC2 among CD11c^{+} CD45R/B220^{-} CD64^{-} cDC; (j) Quantification of CD103^{+} cDC1 purity; (k) Average composition of iDC1 cultures across replicates and experiments; (l) Total numbers of CD103^{+} cDC1 generated per 1 × 10^{6} input bone marrow cells; (m) Representative dot plots showing EdU staining, side scatter, and percentages of EdU^{+} cDC1; (n) Quantification of EdU^{+} cDC1; (o) Representative dot plots showing aCasp3 staining, side scatter, and percentages of aCasp3^{+} cDC1; (p) Quantification of aCasp3^{+} cDC1. ** $p < 0.01$, *** $p < 0.001$, **** $p < 0.0001$ (two-tailed unpaired Student's *t*-test). iDC1: induced cDC1; FLT3L: fms-related tyrosine kinase 3 ligand; cDC1: conventional type 1 dendritic cells; GM-CSF: granulocyte-macrophage colony-stimulating factor; aCasp3: active caspase-3; STAT5: signal transducer and activator of transcription 5; BRD4: bromodomain-containing protein 4; EdU: 5-ethynyl-2′-deoxyuridine.

4. Conclusion

We developed a scalable recombinant cytokine-based BMDC system termed iDC1 that enables efficient generation of highly pure +32 kb *Irf8* enhancer-dependent CD103^{+} cDC1. Compared with existing BMDC methods, and in particular the previously described iCD103-DC protocol, the combination of optimized culture medium, transient KitL supplementation during the early culture phase, and extended culture with serial replating markedly improves cDC1 purity and yield while minimizing contamination by cDC2, macrophages, and other non-DC populations. iDC1 also exhibit phenotypic, transcriptional, and functional properties characteristic of bona fide cDC1, including robust innate responsiveness, IL-12p40 production, and efficient cross-presentation of cell-associated antigen.

Mechanistically, our findings demonstrate that KitL and GM-CSF cooperate during the early stages of cDC1 generation, whereas GM-CSF subsequently maintains differentiated cDC1 through coordinated regulation of survival, proliferation, oxidative stress,

signaling, cytoskeletal remodeling, membrane trafficking, and transcriptional programs. Proteomic and phospho-proteomic analyses further identified STAT5- and BRD4-associated regulatory programs as important contributors to efficient iDC1 generation. Functional analyses further demonstrated that BRD4 deficiency, similar to STAT5 deficiency, reduced cDC1 proliferation and increased apoptosis.

The iDC1 platform should facilitate future studies of cDC1 development, signaling, metabolism, antigen processing, and immunotherapy. In particular, the ability to generate large numbers of pure cDC1 using defined recombinant cytokines may support future preclinical studies investigating cDC1-based vaccination, tumor immunity, and engineered dendritic-cell therapies[6,7,64,65].

Declarations

Acknowledgements

We thank Dr. Dinah Singer for critical reading of the manuscript; Jeffrey Chiang and Jie Mu for technical support; Assiatu Crossman, Kheem Bisht, Don Plugge, William Hajjar, and Tengfei Zhang for flow cytometry support; all staff at the NCI Frederick and NCI Bethesda animal facilities for their critical help. During the preparation of this work, the authors used Claude and ChatGPT provided by the U.S. Department of Health and Human Services in order to optimize language. After using these tools, the authors reviewed and edited the content as needed and take full responsibility for the content of the publication. The content of this publication does not necessarily reflect the views or policies of the Department of Health and Human Services, nor does mention of trade names, commercial products, or organizations imply endorsement by the U.S. Government.

Authors contribution

Sharma S: Investigation, formal analysis, writing-review & editing.
Flynn F, Capaldo B, Holewinski R, Chen Q, Meerzaman D, Andresson T: Investigation, formal analysis.
Mayer CT: Investigation, formal analysis, writing-review & editing, conceptualization, methodology.

Conflicts of interest

The authors declare no conflicts of interest.

Ethical approval

All procedures were approved by the NCI Animal Care and Use Committee (ACUC; #26-056 and EIB-114) and conformed with federal regulatory requirements and standards. The intramural NIH ACU program is accredited by AAALAC International.

Consent to participate

Not applicable.

Consent for publication

Not applicable.

Availability of data and materials

RNA-seq data are available at NCBI Accession PRJNA1474846. Proteomics data are available at MassIVE Accession MSV000101983. Others could be obtained from the corresponding author upon reasonable request.

Funding

This work was supported by the Center for Cancer Research, National Cancer Institute, National Institutes of Health (Grant No. ZIA BC 011975).

Copyright

©The Author(s) 2026.

References

1. Durai V, Murphy KM. Functions of murine dendritic cells. Immunity. 2016;45(4):719-736. [DOI]
2. Hildner K, Edelson BT, Purtha WE, Diamond M, Matsushita H, Kohyama M, et al. Batf3 deficiency reveals a critical role for CD8alpha+ dendritic cells in cytotoxic T cell immunity. Science. 2008;322(5904):1097-1100. [DOI][PubMed][PMC]
3. Mashayekhi M, Sandau MM, Dunay IR, Frickel EM, Khan A, Goldszmid RS, et al. CD8α(+) dendritic cells are the critical source of interleukin-12 that controls acute infection by Toxoplasma gondii tachyzoites. Immunity. 2011;35(2):249-259. [DOI][PubMed][PMC]

4. Koblansky AA, Jankovic D, Oh H, Hieny S, Sungnak W, Mathur R, et al. Recognition of profilin by Toll-like receptor 12 is critical for host resistance to Toxoplasma gondii. Immunity. 2013;38(1):119-130. [DOI][PubMed][PMC]
5. Canton J, Blees H, Henry CM, Buck MD, Schulz O, Rogers NC, et al. The receptor DNGR-1 signals for phagosomal rupture to promote cross-presentation of dead-cell-associated antigens. Nat Immunol. 2021;22(2):140-153. [DOI][PubMed][PMC]
6. Ferris ST, Ohara RA, Ou F, Wu R, Huang X, Kim S, et al. cDC1 vaccines drive tumor rejection by direct presentation independently of host cDC1. Cancer Immunol Res. 2022;10(8):920-931. [DOI]
7. Heras-Murillo I, Mañanes D, Munné P, Núñez V, Herrera J, Catalá-Montoro M, et al. Immunotherapy with conventional type-1 dendritic cells induces immune memory and limits tumor relapse. Nat Commun. 2025;16(1):3369. [DOI][PubMed][PMC]
8. Tussiwand R, Lee WL, Murphy TL, Mashayekhi M, KC W, Albring JC, et al. Compensatory dendritic cell development mediated by BATF-IRF interactions. Nature. 2012;490(7421):502-507. [DOI][PubMed][PMC]
9. Glasmacher E, Agrawal S, Chang AB, Murphy TL, Zeng W, Vander Lugt B, et al. A genomic regulatory element that directs assembly and function of immune-specific AP-1-IRF complexes. Science. 2012;338(6109):975-980. [DOI][PubMed][PMC]
10. Durai V, Bagadia P, Granja JM, Satpathy AT, Kulkarni DH, Davidson IV JT, et al. Cryptic activation of an *Irf8* enhancer governs cDC1 fate specification. Nat Immunol. 2019;20(9):1161-1173. [DOI][PubMed][PMC]
11. Lutz MB, Ali S, Audiger C, Autenrieth SE, Berod L, Bigley V, et al. Guidelines for mouse and human DC generation. Eur J Immunol. 2023;53(11):2249816. [DOI]
12. Helft J, Böttcher J, Chakravarty P, Zelenay S, Huotari J, Schraml BU, et al. GM-CSF mouse bone marrow cultures comprise a heterogeneous population of CD11c(+)MHCII(+) macrophages and dendritic cells. Immunity. 2015;42(6):1197-1211. [DOI][PubMed]
13. Inaba K, Inaba M, Romani N, Aya H, Deguchi M, Ikehara S, et al. Generation of large numbers of dendritic cells from mouse bone marrow cultures supplemented with granulocyte/macrophage colony-stimulating factor. J Exp Med. 1992;176(6):1693-1702. [DOI][PubMed][PMC]
14. Lutz MB, Kukutsch N, Ogilvie AL, Rössner S, Koch F, Romani N, et al. An advanced culture method for generating large quantities of highly pure dendritic cells from mouse bone marrow. J Immunol Methods. 1999;223(1):77-92. [DOI][PubMed]
15. Brasel K, De Smedt T, Smith JL, Maliszewski CR. Generation of murine dendritic cells from flt3-ligand-supplemented bone marrow cultures. Blood. 2000;96(9):3029-3039. [PubMed]
16. Naik SH, O'Keeffe M, Proietto A, Shortman HHK, Wu L. $CD8^+$, $CD8^-$, and plasmacytoid dendritic cell generation *in vitro* using flt3 ligand. Methods Mol Biol. 2010;595:167-176. [DOI][PubMed]
17. Ashayeripanah M, Coughlan H, Zhang S, Yan J, Bandala-Sanchez E, Jenika D, et al. Interleukin 4 selectively expands functional type 1 conventional dendritic cells from bone marrow progenitors. Cell Rep. 2026;45(1):116772. [DOI]
18. Kirkling ME, Cytlak U, Lau CM, Lewis KL, Resteu A, Khodadadi-Jamayran A, et al. Notch signaling facilitates *in vitro* generation of cross-presenting classical dendritic cells. Cell Rep. 2018;23(12):3658-3672.e6. [DOI]
19. Mayer CT, Ghorbani P, Nandan A, Dudek M, Arnold-Schrauf C, Hesse C, et al. Selective and efficient generation of functional Batf3-dependent $CD103^+$ dendritic cells from mouse bone marrow. Blood. 2014;124(20):3081-3091. [DOI][PubMed][PMC]
20. Ou F, Ferris ST, Kim S, Wu R, Anderson DA III, Liu TT, et al. Enhanced *in vitro* type 1 conventional dendritic cell generation via the recruitment of hematopoietic stem cells and early progenitors by Kit ligand. Eur J Immunol. 2023;53(9):2250201. [DOI]
21. Cyran L, Serfling J, Kirschner L, Raifer H, Lohoff M, Hermanns HM, et al. Flt3L, LIF, and IL-10 combination promotes the selective *in vitro* development of $ESAM^{low}$ cDC2B from murine bone marrow. Eur J Immunol. 2022;52(12):1946-1960. [DOI][PubMed]
22. Ferris ST, Durai V, Wu R, Theisen DJ, Ward JP, Bern MD, et al. cDC1 prime and are licensed by $CD4^+$ T cells to induce anti-tumour immunity. Nature. 2020;584(7822):624-629. [DOI][PubMed][PMC]
23. Schwenk F, Baron U, Rajewsky K. A cre-transgenic mouse strain for the ubiquitous deletion of loxP-flanked gene segments including deletion in germ cells. Nucleic Acids Res. 1995;23(24):5080-5081. [DOI][PubMed][PMC]
24. Knittel G, Liedgens P, Korovkina D, Seeger JM, Al-Baldawi Y, Al-Maarri M, et al. B-cell-specific conditional expression of Myd88p.L252P leads to the development of diffuse large B-cell lymphoma in mice. Blood. 2016;127(22):2732-2741. [DOI]
25. Mayer CT, Gazumyan A, Kara EE, Gitlin AD, Golijanin J, Viant C, et al. The microanatomic segregation of selection by apoptosis in the germinal center. Science. 2017;358(6360):eaao2602. [DOI][PubMed][PMC]
26. Cui Y, Riedlinger G, Miyoshi K, Tang W, Li C, Deng CX, et al. Inactivation of Stat5 in mouse mammary epithelium during pregnancy reveals distinct functions in cell proliferation, survival, and differentiation. Mol Cell Biol. 2004;24(18):8037-8047. [DOI][PubMed][PMC]
27. Devaiah BN, Case-Borden C, Gegonne A, Hsu CH, Chen Q, Meerzaman D, et al. BRD4 is a histone acetyltransferase that evicts nucleosomes from chromatin. Nat Struct Mol Biol. 2016;23(6):540-548. [DOI][PubMed][PMC]
28. Hogquist KA, Jameson SC, Heath WR, Howard JL, Bevan MJ, Carbone FR. T cell receptor antagonist peptides induce positive selection. Cell. 1994;76(1):17-27. [DOI]
29. Barnden MJ, Allison J, Heath WR, Carbone FR. Defective TCR expression in transgenic mice constructed using cDNA-based alpha- and beta-chain genes under the control of heterologous regulatory elements. Immunol Cell Biol. 1998;76(1):34-40. [DOI][PubMed]
30. Koller BH, Marrack P, Kappler JW, Smithies O. Normal development of mice deficient in β_2M, MCClass I proteins, and $CD8^+$ T cells. Science. 1990;248(4960):1227-1230. [DOI]
31. Mort RL, Ford MJ, Sakaue-Sawano A, Lindstrom NO, Casadio A, Douglas AT, et al. Fucci2a: A bicistronic cell cycle reporter that allows Cre mediated tissue specific expression in mice. Cell Cycle. 2014;13(17):2681-2696. [DOI][PubMed][PMC]
32. Von Boehmer L, Liu C, Ackerman S, Gitlin AD, Wang Q, Gazumyan A, et al. Sequencing and cloning of antigen-specific antibodies from

mouse memory B cells. Nat Protoc. 2016;11(10):1908-1923. [DOI][PubMed]
33. Simpson MJ, Newen AM, McNees C, Sharma S, Pfannenstiel D, Moyer T, et al. Peripheral apoptosis and limited clonal deletion during physiologic murine B lymphocyte development. Nat Commun. 2024;15(1):4691. [DOI][PubMed][PMC]
34. Soneson C, Love MI, Robinson MD. Differential analyses for RNA-seq: Transcript-level estimates improve gene-level inferences. F1000Res. 2015;4:1521. [DOI][PubMed][PMC]
35. Chen Y, Chen L, Lun ATL, Baldoni PL, Smyth GK. edgeR v4: Powerful differential analysis of sequencing data with expanded functionality and improved support for small counts and larger datasets. Nucleic Acids Res. 2025;53(2):gkaf018. [DOI]
36. Chen Y, Lun ATL, Smyth GK. From reads to genes to pathways: Differential expression analysis of RNA-Seq experiments using Rsubread and the edgeR quasi-likelihood pipeline. F1000Res. 2016;5:1438. [DOI][PubMed][PMC]
37. Ritchie ME, Phipson B, Wu D, Hu Y, Law CW, Shi W, et al. Limma powers differential expression analyses for RNA-sequencing and microarray studies. Nucleic Acids Res. 2015;43(7):e47. [DOI][PubMed][PMC]
38. Hoffman GE, Roussos P. Dream: Powerful differential expression analysis for repeated measures designs. Bioinformatics. 2021;37(2):192-201. [DOI][PubMed][PMC]
39. Hoffman GE, Schadt EE. variancePartition: Interpreting drivers of variation in complex gene expression studies. BMC Bioinformatics. 2016;17(1):483. [DOI][PubMed][PMC]
40. Xu S, Hu E, Cai Y, Xie Z, Luo X, Zhan L, et al. Using clusterProfiler to characterize multiomics data. Nat Protoc. 2024;19(11):3292-3320. [DOI]
41. Aran D, Looney AP, Liu L, Wu E, Fong V, Hsu A, et al. Reference-based analysis of lung single-cell sequencing reveals a transitional profibrotic macrophage. Nat Immunol. 2019;20(2):163-172. [DOI][PubMed][PMC]
42. Kim J, Nguyen T, Cifello J, Ahmad R, Zhang Y, Yang Q, et al. Lysine methyltransferase Kmt2d regulates naive $CD8^+$ T cell activation-induced survival. Front Immunol. 2022;13:1095140. [DOI][PubMed][PMC]
43. Becattini S, Littmann ER, Seok R, Amoretti L, Fontana E, Wright R, et al. Enhancing mucosal immunity by transient microbiota depletion. Nat Commun. 2020;11(1):4475. [DOI][PubMed][PMC]
44. Schnorrer P, Behrens GMN, Wilson NS, Pooley JL, Smith CM, El-Sukkari D, et al. The dominant role of $CD8^+$ dendritic cells in cross-presentation is not dictated by antigen capture. Proc Natl Acad Sci U S A. 2006;103(28):10729-10734. [DOI][PubMed][PMC]
45. Sathaliyawala T, O'Gorman WE, Greter M, Bogunovic M, Konjufca V, Hou ZE, et al. Mammalian target of rapamycin controls dendritic cell development downstream of Flt3 ligand signaling. Immunity. 2010;33(4):597-606. [DOI][PubMed][PMC]
46. Böttcher JP, Bonavita E, Chakravarty P, Blees H, Cabeza-Cabrerizo M, Sammicheli S, et al. NK cells stimulate recruitment of cDC1 into the tumor microenvironment promoting cancer immune control. Cell. 2018;172(5):1022-1037.e14. [DOI][PubMed][PMC]
47. Ferry A, Mempel KM, Monell A, Reina-Campos M, Scharping NE, Heeg M, et al. The XCL1-XCR1 axis supports intestinal tissue residency and antitumor immunity. J Exp Med. 2025;222(2):e20240776. [DOI][PubMed][PMC]
48. Miller JC, Brown BD, Shay T, Gautier EL, Jojic V, Cohain A, et al. Deciphering the transcriptional network of the dendritic cell lineage. Nat Immunol. 2012;13(9):888-899. [DOI][PubMed][PMC]
49. Balan S, Ollion V, Colletti N, Chelbi R, Montanana-Sanchis F, Liu H, et al. Human $XCR1^+$ dendritic cells derived *in vitro* from $CD34^+$ progenitors closely resemble blood dendritic cells, including their adjuvant responsiveness, contrary to monocyte-derived dendritic cells. J Immunol. 2014;193(4):1622-1635. [DOI]
50. Poulin LF, Salio M, Griessinger E, Anjos-Afonso F, Craciun L, Chen JL, et al. Characterization of human $DNGR\text{-}1^+$ $BDCA3^+$ leukocytes as putative equivalents of mouse $CD8alpha^+$ dendritic cells. J Exp Med. 2010;207(6):1261-1271. [DOI][PubMed][PMC]
51. Proietto AI, Mittag D, Roberts AW, Sprigg N, Wu L. The equivalents of human blood and spleen dendritic cell subtypes can be generated *in vitro* from human $CD34^+$ stem cells in the presence of fms-like tyrosine kinase 3 ligand and thrombopoietin. Cell Mol Immunol. 2012;9(6):446-454. [DOI][PubMed][PMC]
52. Balan S, O'Brien L, Peros A, Wang X, Leal Rojas I, McClain C, et al. Harnessing Notch signaling to enhance the generation and functionality of human conventional type 1 dendritic cells for cancer immunotherapy applications. Cancer Immunol Res. 2025;13(9):1328-1341. [DOI][PubMed]
53. Liu C, Bi S, Chen W, Tian Y, Li H, Li G, et al. Scalable generation of clinical-grade universal human cDC1s enables potent antitumor immunotherapy. bioRxiv [Preprint]. 2026. [DOI]
54. Swartz AM, Nair SK. The *in vitro* differentiation of human $CD141^+CLEC9A^+$ dendritic cells from mobilized peripheral blood $CD34^+$ hematopoietic stem cells. Curr Protoc. 2022;2(4):e410. [DOI]
55. Zhan Y, Carrington EM, van Nieuwenhuijze A, Bedoui S, Seah S, Xu Y, et al. GM-CSF increases cross-presentation and CD103 expression by mouse $CD8^+$ spleen dendritic cells. Eur J Immunol. 2011;41(9):2585-2595. [DOI]
56. Sathe P, Pooley J, Vremec D, Mintern J, Jin JO, Wu L, et al. The acquisition of antigen cross-presentation function by newly formed dendritic cells. J Immunol. 2011;186(9):5184-5192. [DOI]
57. de Brito C, Tomkowiak M, Ghittoni R, Caux C, Leverrier Y, Marvel J. CpG promotes cross-presentation of dead cell-associated antigens by pre-CD8α+ dendritic cells. J Immunol. 2011;186(3):1503-1511. [DOI][PubMed]
58. Shiomi A, Usui T. Pivotal roles of GM-CSF in autoimmunity and inflammation. Mediators Inflamm. 2015;2015:568543. [DOI][PubMed][PMC]
59. Van de Laar L, Coffer PJ, Woltman AM. Regulation of dendritic cell development by GM-CSF: Molecular control and implications for immune homeostasis and therapy. Blood. 2012;119(15):3383-3393. [DOI][PubMed]

60. KC W, Satpathy AT, Rapaport AS, Briseño CG, Wu X, Albring JC, et al. L-Myc expression by dendritic cells is required for optimal T-cell priming. Nature. 2014;507(7491):243-247. [DOI][PubMed][PMC]
61. Devaiah BN, Mu J, Akman B, Uppal S, Weissman JD, Cheng D, et al. MYC protein stability is negatively regulated by BRD4. Proc Natl Acad Sci U S A. 2020;117(24):13457-13467. [DOI][PubMed][PMC]
62. Eddy WE, Gong KQ, Bell B, Parks WC, Ziegler SF, Manicone AM. Stat5 is required for CD103^{+} dendritic cell and alveolar macrophage development and protection from lung injury. J Immunol. 2017;198(12):4813-4822. [DOI][PubMed][PMC]
63. Li HS, Yang CY, Nallaparaju KC, Zhang H, Liu YJ, Goldrath AW, et al. The signal transducers STAT5 and STAT3 control expression of Id2 and E2-2 during dendritic cell development. Blood. 2012;120(22):4363-4373. [DOI][PubMed][PMC]
64. Ward RW, Kar U, Balan S, Bhardwaj N. Leveraging cDC1 biology and function for enhanced immunotherapy. J Exp Med. 2026;223(7):e20241199. [DOI]
65. Wculek SK, Cueto FJ, Mujal AM, Melero I, Krummel MF, Sancho D. Dendritic cells in cancer immunology and immunotherapy. Nat Rev Immunol. 2020;20(1):7-24. [DOI]

Publisher's Note

Science Exploration remains a neutral stance on jurisdictional claims in published maps and institutional affiliations. The views expressed in this article are solely those of the author(s) and do not reflect the opinions of the Editors or the publisher.